Journal of Computational Physics 228 (2009) 4055–4087

Contents lists available at ScienceDirect

Journal of Computational Physics

journal homepage: www.elsevier.com/locate/jcp

A novel Galerkin-like weakform and a superconvergent alpha finite element method (SαFEM) for mechanics problems using triangular meshes

G.R. Liu [a,b], H. Nguyen-Xuan [a,c,*], T. Nguyen-Thoi [b,c], X. Xu [b]

[a] Singapore-MIT Alliance (SMA), E4-04-10, 4 Engineering Drive 3, Singapore 117576, Singapore
[b] Center for Advanced Computations in Engineering Science (ACES), Department of Mechanical Engineering, National University of Singapore, 9 Engineering Drive 1, Singapore 117576, Singapore
[c] Department of Mechanics, Faculty of Mathematics and Computer Science, University of Science HCM, Vietnam National University, Vietnam

ARTICLE INFO

Article history:
Received 4 September 2008
Received in revised form 17 January 2009
Accepted 13 February 2009
Available online 26 February 2009

Keywords:
Numerical methods
Meshfree methods
Finite element method (FEM)
Alpha finite element method (αFEM)
Node-based smoothed finite element method (NS-FEM)
Solution bounds
Superconvergence
Strain construction methods

ABSTRACT

A carefully designed procedure is presented to modify the piecewise constant strain field of linear triangular FEM models, and to reconstruct a strain field with an adjustable parameter α. A novel Galerkin-like weakform derived from the Hellinger–Reissner variational principle is proposed for establishing the discretized system equations. The new weak form is very simple, possesses the same good properties of the standard Galerkin weakform, and works particularly well for strain construction methods. A superconvergent alpha finite element method (SαFEM) is then formulated by using the constructed strain field and the Galerkin-like weakform for solid mechanics problems. The implementation of the SαFEM is straightforward and no additional parameters are used. We prove theoretically and show numerically that the SαFEM always achieves more accurate and higher convergence rate than the standard FEM of triangular elements (T3) and even more accurate than the four-node quadrilateral elements (Q4) when the same sets of nodes are used. The SαFEM can always produce both lower and upper bounds to the exact solution in the energy norm for all elasticity problems by properly choosing an α. In addition, a preferable-α approach has also been devised to produce very accurate solutions for both displacement and energy norms and a superconvergent rate in the energy error norm. Furthermore, a model-based selective scheme is proposed to formulate a combined SαFEM/NS-FEM model that handily overcomes the volumetric locking problems. Intensive numerical studies including singularity problems have been conducted to confirm the theory and properties of the SαFEM.

© 2009 Elsevier Inc. All rights reserved.

1. Introduction

The finite element method (FEM) has become a very powerful and reliable tool for numerical simulations in engineering and science [1–3]. Commercial software packages are now widely used in engineering design of structural systems due to their versatility for complicated geometries and non-linear problems. In practical applications, the lower-order linear triangular element is preferred to many engineers due to its simplicity, efficiency, robustness, less demand on the smoothness of the solution, and easy for adaptive mesh refinements for solutions of desired accuracy. However, the fully-compatible FEM

* Corresponding author. Address: Singapore-MIT Alliance (SMA), E4-04-10, 4 Engineering Drive 3, Singapore 117576, Singapore. Tel.: +65 9860 4962.
E-mail addresses: smanxh@nus.edu.sg, nxhung@hcmuns.edu.vn (H. Nguyen-Xuan).

0021-9991/$ - see front matter © 2009 Elsevier Inc. All rights reserved.
doi:10.1016/j.jcp.2009.02.017

model using 3-node triangular element (T3) has certain inherent drawbacks: (1) overestimation of stiffness matrix [4,5] especially for problems with locking behavior; (2) poor performance when distorted meshes are used; (3) poor accuracy in the stress results. One of the attempts in improving the constant strain triangular element is to add an in-plane rotational degree of freedom which was initially proposed by Allman [6]. Various improvements of formulations as well as numerical techniques on the rotational degree of freedom have then been performed [7–11]. The concept of enhanced strains introduced by Simo and Rifai [12] has been developed by many authors to improve the performance of low order finite elements [10,13–18]. The assumed stress element [19] was also proposed to solve locking problems.

On the other front of the development, Liu et al. [20] has formulated the linear conforming point interpolation method (LC-PIM) using PIM shape functions constructed with a set of small number of nodes chosen in a local support domain that can overlap [21,22]. A generalized strain smoothing technique [5] has been proposed based on the strain smoothing technique [23]. The generalized strain smoothing technique forms a foundation of unified formulations for both incompatible and compatible displacement methods. Because the node-based smoothing operation is used in the LC-PIM, it is also termed as a node-based smoothed point interpolation method (NS-PIM). Introducing the strain smoothing operation into the finite elements, the element-based smoothed finite element method (SFEM) [24] has also been formulated. The theoretical base of SFEM was then established and proven in detail in [25,26]. The SFEM has also been developed for general n-sided polygonal elements (nSFEM) [27], dynamic analyses [28], plate and shell analyses [29–32]. Strain smoothing has recently been coupled to the extended finite element method (XFEM) [33–35] and partition of unity method [36,37] to solve fracture mechanics problems in 2D continuum and plates, e.g. [38]. This coupling is very promising to create a flexible extended finite element method (FleXFEM) [38].

Based on the idea of the NS-PIM and the SFEM, a node-based smoothed finite element method (NS-FEM) [39] for 2D solid mechanics problems has been developed. It was shown that NS-PIM and NS-FEM work very well in solving the volumetric locking problems. They are also less sensitive to mesh distortion, and achieve more accurate stress solutions when triangular elements are used. Furthermore, both the NS-PIM and NS-FEM can provide an upper bound [39,40] to exact solution in the strain energy for elasticity problems with non-zero external forces [41,42]. However, it is also found that both NS-PIM and NS-FEM models can lead to spurious non-zero energy modes for dynamic problems, due to an "overly-soft" behavior that is in contrary to the "overly-stiff" phenomenon of the standard compatible FEM (T3) [4,5]. The overly-soft behavior can be overcome by using a stabilized technique in the nodal integration methods [43,44]. And an effective cure is to use the edge-based smoothed finite element method (ES-FEM) [45] which possesses a very "close-to-exact" stiffness and has not spurious non-zero energy modes. The ES-FEM therefore can give very accurate, stable and superconvergent solutions to both static and dynamic problems.

The finite element methods with free parameters have been well known via previous contributions in [46–49]. An alpha finite element method (αFEM) [50] using quadrilateral elements was recently formulated to obtain "nearly exact" or best possible solution for a given problem by scaling the gradient of strains in the natural coordinates and Jacobian matrices with a scaling factor α. The method is not variationally consistent but proven stable and convergent. The αFEM can produce approximate solutions that are "very close to exact" solutions in the strain energy for all overestimation problems, and the "best" possible solution to underestimation problems. An αFEM using triangular and tetrahedral elements for exact solution to mechanics problems has also been proposed [51]. Along with the idea of the αFEM [50], a variationally consistent αFEM (VCαFEM) [52] has also been formulated by scaling only the gradient of strain in the physical coordinates, without scaling the Jacobian matrix, and using the Hellinger–Reissner variational principle. The VCαFEM can produce both lower and upper bounds to the exact solution in energy norm for all problems of elasticity by properly choosing the scaling factor α. The important bound property is then used to device an exact-α approach for ultra-accurate solutions that are very close to the exact solution in the energy norm. Furthermore, the VCαFEM can also perform well for problems with volumetric locking through the incorporation with a stabilization technique [53,54]. Following the idea of αFEM, a superconvergent point interpolation method (SC-PIM) [55] using triangular meshes and the piecewise constant strain field has also been developed for superconvergent solutions in meshfree methods [56–64].

In this paper, a superconvergent alpha finite element method (SαFEM) using triangular meshes is proposed. A strain field is carefully constructed by combining the compatible strains and the averaged nodal strains with an adjustable factor α. A novel variationally consistent Galerkin-like weak form for the SαFEM is derived from the Hellinger–Reissner variational principle. Due to the particular way of the strain field constructed, the new Galerkin-like weak form is as simple as the Galerkin weak form and the resultant stiffness matrix is symmetric. We prove theoretically and show numerically that the SαFEM is much more accurate than the original FEM-T3 and even more accurate than the FEM-Q4 when the same sets of nodes are used. The SαFEM can produce both lower and upper bounds to the exact solution in the energy norm for all elasticity problems by properly choosing an α. In addition, a preferable-α approach has also been devised for the SαFEM to produce very accurate solutions for both displacement and energy norms and the superconvergent rate in the energy error norm. Furthermore, a model-based selective scheme is proposed to formulate a combined SαFEM/NS-FEM model that handily overcomes the volumetric locking problems. Intensive numerical studies including two singularity problems have been conducted to confirm the theory and properties of the SαFEM.

The paper is outlined as follows. In Section 2, an assumed strain field based on linear triangular element (T3) is introduced. In Section 3, the variational principle is used to formulate the SαFEM. Some theoretical properties of the SαFEM are presented and proven in Section 4. Section 5 presents a combined SαFEM/NS-FEM model for free of volumetric locking. Section 6 briefs the numerical implementation procedure. The procedure of determining the preferable α for the supercon-

vergent solution is introduced in Section 7. Section 8 presents and discusses numerical results. Computational efficiency and condition number of the SαFEM are resulted in Section 9. Section 10 closes some concluding remarks.

2. Construction of an assumed strain field

The problem domain Ω is first divided into a set of triangular mesh with N nodes and N_e elements. We then divide, in a overlay fashion, the domain into a set of smoothing domains Ω_k, $k = 1, 2, \ldots, N$, by connecting node k to centroids of the surrounding triangles as shown in Fig. 1. The smoothing domain Ω_k is further subdivided into M sub-domains $\Omega_{k,i}$ as shown in Fig. 2 such as $\Omega_k = \bigcup_{i=1}^{M} \Omega_{k,i}, \Omega_{k,i} \cap \Omega_{k,j} = \emptyset, i \neq j$.

The approximation of the displacement $\hat{\mathbf{u}} = (u_x^h, u_y^h)$ of the elasticity problem can be then expressed as

$$\hat{\mathbf{u}}(\mathbf{x}) = \sum_{I=1}^{np} N_I(\mathbf{x}) \hat{\mathbf{d}}_I \tag{1}$$

where np is the total number of nodes in the mesh, $\hat{\mathbf{d}}_I$ is the vector of nodal displacements and

$$N_I(\mathbf{x}) = \begin{bmatrix} N_I(\mathbf{x}) & 0 \\ 0 & N_I(\mathbf{x}) \end{bmatrix} \tag{2}$$

is the matrix of the FEM shape functions for node I created based on the elements.

In the previous work on the VCαFEM formulation [52], an assumed strain constructed for quadrilateral meshes is based on the compatible strain and an additional strain. As a result, a simple and effective form of stiffness matrix expressed similarly to a stabilized approach [53,54,65] is then obtained. However, such a formulation is only for quadrilateral elements. It does not work for triangular elements because the strain in triangular elements is constant and there is no room for maneuver within the elements. In this work, we try to create such a simple formula for triangular meshes that works well for complicated geometries. To obtain this, we need to *properly* bring in information from the neighbouring triangular elements. Our procedure is as follows:

First, the compatible strain $\tilde{\boldsymbol{\varepsilon}}_{k,i}$ at any point using the assumed displacement field based on triangular elements is used

$$\tilde{\boldsymbol{\varepsilon}}_{k,i} = \nabla_s \hat{\mathbf{u}}_{k,i}(\mathbf{x}) \tag{3}$$

where ∇_s is a differential operator matrix given by

$$\nabla_s = \begin{bmatrix} \frac{\partial}{\partial x} & 0 & \frac{\partial}{\partial y} \\ 0 & \frac{\partial}{\partial y} & \frac{\partial}{\partial x} \end{bmatrix}^T \tag{4}$$

Because the displacement is linear, $\tilde{\boldsymbol{\varepsilon}}_{k,i}$ is constant in $\Omega_{k,i}$ and different from element to element. Such a piecewise constant strain field obviously does not represent well the exact strain field, and should be somehow modified or corrected. To make a proper correction, a smoothed strain for node k (see, Fig. 2) is introduced as follows:

$$\bar{\boldsymbol{\varepsilon}}_k = \frac{1}{A_k} \int_{\Omega_k} \tilde{\boldsymbol{\varepsilon}}_{k,i}(\mathbf{x}) d\Omega \tag{5}$$

where A_k is the area of smoothing domain Ω_k.

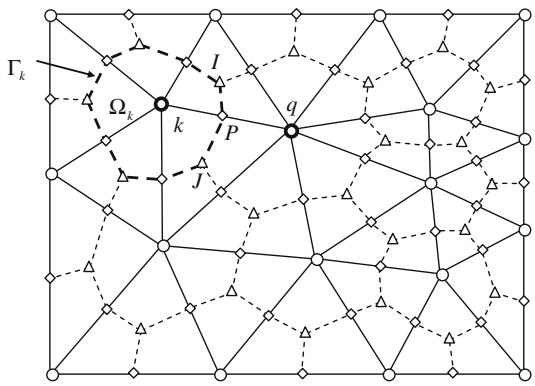

○ Field node (k, q); ◇ Mid-edge-point (P); △ Centroid of triangle (I, J)

Fig. 1. Triangular elements and smoothing cells associated to nodes.

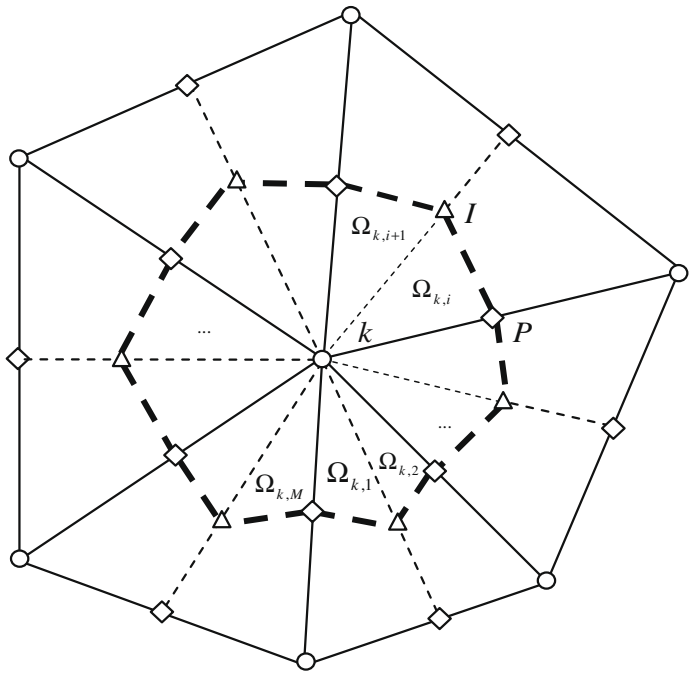

Fig. 2. Smoothing cell and triangular sub-domains associated with node k.

The strains $\boldsymbol{\varepsilon}_P$, $\boldsymbol{\varepsilon}_I$ at points P, I are then assigned as

$$\begin{aligned}
\boldsymbol{\varepsilon}_P &= \boldsymbol{\varepsilon}_I = \tilde{\boldsymbol{\varepsilon}}_{k,i} - \frac{\alpha\sqrt{6}}{3}(\bar{\boldsymbol{\varepsilon}}_k - \tilde{\boldsymbol{\varepsilon}}_{k,i}) \\
\boldsymbol{\varepsilon}_k &= \alpha\sqrt{6}\bar{\boldsymbol{\varepsilon}}_k + (1-\alpha\sqrt{6})\tilde{\boldsymbol{\varepsilon}}_{k,i} - \frac{\alpha\sqrt{6}}{3}(\bar{\boldsymbol{\varepsilon}}_k - \tilde{\boldsymbol{\varepsilon}}_{k,i}), \quad \forall\alpha \in \mathbb{R}
\end{aligned} \tag{6}$$

where α is an adjustable factor. The strain field $\hat{\boldsymbol{\varepsilon}}$ at any points within a sub-triangular domain $\Omega_{k,i}$ is now re-constructed as [55]

$$\begin{aligned}
\hat{\boldsymbol{\varepsilon}}(\mathbf{x}) &= L_1(\mathbf{x})\boldsymbol{\varepsilon}_k + L_2(\mathbf{x})\boldsymbol{\varepsilon}_P + L_3(\mathbf{x})\boldsymbol{\varepsilon}_I \\
&= L_1(\mathbf{x})\left(\alpha\sqrt{6}\bar{\boldsymbol{\varepsilon}}_k + \left(1-\alpha\sqrt{6}\right)\tilde{\boldsymbol{\varepsilon}}_{k,i} - \frac{\sqrt{6}}{3}\alpha(\bar{\boldsymbol{\varepsilon}}_k - \tilde{\boldsymbol{\varepsilon}}_{k,i})\right) + L_2(\mathbf{x})\left(\tilde{\boldsymbol{\varepsilon}}_{k,i} - \frac{\sqrt{6}}{3}\alpha(\bar{\boldsymbol{\varepsilon}}_k - \tilde{\boldsymbol{\varepsilon}}_{k,i})\right) \\
&\quad + L_3(\mathbf{x})\left(\tilde{\boldsymbol{\varepsilon}}_{k,i} - \frac{\sqrt{6}}{3}\alpha(\bar{\boldsymbol{\varepsilon}}_k - \tilde{\boldsymbol{\varepsilon}}_{k,i})\right)
\end{aligned} \tag{7}$$

where L_1, L_2, L_3 is the area coordinates for the sub-triangular $\Omega_{k,i}$, which are partitions of unity. Eq. (7) can be simplified as

$$\hat{\boldsymbol{\varepsilon}}(\mathbf{x}) = \underbrace{(L_1 + L_2 + L_3)}_{1}\tilde{\boldsymbol{\varepsilon}}_{k,i} + \alpha\sqrt{6}L_1(\mathbf{x})(\bar{\boldsymbol{\varepsilon}}_k - \tilde{\boldsymbol{\varepsilon}}_{k,i}) - \underbrace{(L_1 + L_2 + L_3)}_{1}\alpha\frac{\sqrt{6}}{3}(\bar{\boldsymbol{\varepsilon}}_k - \tilde{\boldsymbol{\varepsilon}}_{k,i}) \tag{8}$$

which can be simplified as

$$\hat{\boldsymbol{\varepsilon}}(\mathbf{x}) = \tilde{\boldsymbol{\varepsilon}}_{k,i} + \alpha\boldsymbol{\varepsilon}^{ad}_{k,i}(\mathbf{x}) \tag{9}$$

where $\tilde{\boldsymbol{\varepsilon}}_{k,i}$ is constant in $\Omega_{k,i}$ and

$$\boldsymbol{\varepsilon}^{ad}_{k,i}(\mathbf{x}) = \sqrt{6}(\bar{\boldsymbol{\varepsilon}}_k - \tilde{\boldsymbol{\varepsilon}}_{k,i})\left(L_1(\mathbf{x}) - \frac{1}{3}\right) \tag{10}$$

which is the "adjusted" strain. It is a linear function representing the variation of the re-constructed strain field in $\Omega_{k,i}$. It is clear that we have successfully constructed a linear strain field in $\Omega_{k,i}$ without adding any degrees of freedoms. We now need to examine the "legality" of the constructed strain field.

Using the formula [2,3],

$$\int_{A_{k,i}} L_1^p L_2^q L_3^r \, dA = \frac{p!q!r!}{(p+q+r+2)!} 2A_{k,i} \tag{11}$$

it is easy to prove that

$$\int_{\Omega_{k,i}} \boldsymbol{\varepsilon}_{k,i}^{ad} \, d\Omega = \sqrt{6}(\bar{\boldsymbol{\varepsilon}}_k - \tilde{\boldsymbol{\varepsilon}}_{k,i}) \int_{\Omega_{k,i}} \left(L_1 - \frac{1}{3} \right) d\Omega = 0 \tag{12}$$

which is termed as zero-sum property of the correction strain, which is similar to orthogonal condition that used in the stabilization formulation [53,54,65]. The zero-sum property results in the following total zero-sum of the additional strain over the entire problem domain:

$$\int_{\Omega} \boldsymbol{\varepsilon}^{ad} \, d\Omega = \sum_{k=1}^{N} \sum_{i=1}^{M} \int_{\Omega_{k,i}} \boldsymbol{\varepsilon}_{k,i}^{ad} \, d\Omega = \mathbf{0} \tag{13}$$

Therefore, we shall have

$$\int_{\Omega} \hat{\boldsymbol{\varepsilon}} \, d\Omega = \int_{\Omega} \tilde{\boldsymbol{\varepsilon}} \, d\Omega + \underbrace{\int_{\Omega} \boldsymbol{\varepsilon}^{ad} \, d\Omega}_{=0} = \sum_{k=1}^{N} \sum_{i=1}^{M} \int_{\Omega_{k,i}} \tilde{\boldsymbol{\varepsilon}}_{k,i} \, d\Omega \tag{14}$$

which implies that the strain $\boldsymbol{\varepsilon}_{k,i}^{ad}$ does not effect on the constant stress state that is needed to satisfy a patch test [10,12], and hence ensures the convergence. The zero-sum Eq. (12) as shown later is also important to simplify the formulation.

It is clear now that the key idea of this work is to re-construct carefully strain field $\hat{\boldsymbol{\varepsilon}}$ using the constant compatible strains $\tilde{\boldsymbol{\varepsilon}}$ of the FEM and the node-based smoothed strains $\bar{\boldsymbol{\varepsilon}}$ of the NS-FEM, so that SαFEM can always pass the standard patch tests ensuring the convergence. In addition, we introduce an α to regularize the variation of the strain field. Based on the findings in [50] that the gradient of strain field can be "freely" scaled as long as the zero-sum property is maintained, the SαFEM will converge for any $\alpha \in \mathbb{R}$. We now have a "knob" to tune for desired solutions such as upper and lower bounds to the exact solution and superconvergent solutions. Note that the reconstruction of the strain field is very simple. The process does not add any degrees of freedom, and all the standard FEM procedure is almost unchanged. For incompressible problems, we further propose a novel technique that combines the SαFEM and the NS-FEM approach to overcome volumetric locking.

3. Weak form for modified strain field

Property 1. *The following Galerkin-like weakform*

$$\sum_{k=1}^{N} \sum_{i=1}^{M} \left[\int_{\Omega_{k,i}} \delta \left(\tilde{\boldsymbol{\varepsilon}}_{k,i} + \alpha \boldsymbol{\varepsilon}_{k,i}^{ad} \right)^T \mathbf{D} \left(\tilde{\boldsymbol{\varepsilon}}_{k,i} - \alpha \boldsymbol{\varepsilon}_{k,i}^{ad} \right) d\Omega \right] - \int_{\Omega} \delta \mathbf{u}^T \mathbf{b} \, d\Omega - \int_{\Gamma_t} \delta \mathbf{u}^T \bar{\mathbf{t}} \, d\Gamma = 0 \tag{15}$$

with the constructed strain field given by Eq. (9) is variationally consistent for elasticity problems.

Proof. In the present formulation, the usual compatible strain field is replaced by the modified strain field by Eq. (9), and hence the modified Hellinger–Reissner variational principle with the assumed strain vector $\hat{\boldsymbol{\varepsilon}}$ and displacement field $\hat{\mathbf{u}}$ as independent field variables for elasticity problems can be used [19]

$$\Pi_{HR}(\hat{\mathbf{u}}, \hat{\boldsymbol{\varepsilon}}) = -\frac{1}{2} \int_{\Omega} \hat{\boldsymbol{\varepsilon}}^T \mathbf{D} \hat{\boldsymbol{\varepsilon}} \, d\Omega + \int_{\Omega} \hat{\boldsymbol{\varepsilon}}^T \mathbf{D} \tilde{\boldsymbol{\varepsilon}} \, d\Omega - \int_{\Omega} \mathbf{u}^T \mathbf{b} \, d\Omega - \int_{\Gamma_t} \mathbf{u}^T \bar{\mathbf{t}} \, d\Gamma \tag{16}$$

The strain energy is given by

$$\hat{U}(\hat{\mathbf{u}}) = -\frac{1}{2} \int_{\Omega} \hat{\boldsymbol{\varepsilon}}^T \mathbf{D} \hat{\boldsymbol{\varepsilon}} \, d\Omega + \int_{\Omega} \hat{\boldsymbol{\varepsilon}}^T \mathbf{D} \tilde{\boldsymbol{\varepsilon}} \, d\Omega \tag{17}$$

which can be rewritten in a summation of integrals for all sub-domain $\Omega_{k,i}$

$$\hat{U}(\hat{\mathbf{u}}) = \sum_{k=1}^{N} \sum_{i=1}^{M} \left[-\frac{1}{2} \int_{\Omega_{k,i}} \hat{\boldsymbol{\varepsilon}}_{k,i}^T \mathbf{D} \hat{\boldsymbol{\varepsilon}}_{k,i} \, d\Omega + \int_{\Omega_{k,i}} \hat{\boldsymbol{\varepsilon}}_{k,i}^T \mathbf{D} \tilde{\boldsymbol{\varepsilon}}_{k,i} \, d\Omega \right] = \sum_{k=1}^{N} \sum_{i=1}^{M} \hat{U}_{k,i}(\hat{\mathbf{u}}) \tag{18}$$

where

$$\hat{U}_{k,i}(\hat{\mathbf{u}}) = -\frac{1}{2} \int_{\Omega_{k,i}} \hat{\boldsymbol{\varepsilon}}_{k,i}^T \mathbf{D} \hat{\boldsymbol{\varepsilon}}_{k,i} \, d\Omega + \int_{\Omega_{k,i}} \hat{\boldsymbol{\varepsilon}}_{k,i}^T \mathbf{D} \tilde{\boldsymbol{\varepsilon}}_{k,i} \, d\Omega \tag{19}$$

Substituting Eq. (7) into Eq. (19) leads to

$$\begin{aligned}\widehat{U}_{k,i}(\hat{\mathbf{u}},\alpha) &= -\frac{1}{2}\int_{\Omega_{k,i}}(\tilde{\boldsymbol{\varepsilon}}_{k,i}+\alpha\boldsymbol{\varepsilon}^{ad}_{k,i})^T\mathbf{D}(\boldsymbol{\varepsilon}_{k,i}+\alpha\boldsymbol{\varepsilon}^{ad}_{k,i})d\Omega+\int_{\Omega_{k,i}}(\tilde{\boldsymbol{\varepsilon}}_{k,i}+\alpha\boldsymbol{\varepsilon}^{ad}_{k,i})^T\mathbf{D}\tilde{\boldsymbol{\varepsilon}}_{k,i}\,d\Omega\\
&= -\frac{1}{2}\int_{\Omega_{k,i}}\tilde{\boldsymbol{\varepsilon}}^T_{k,i}\mathbf{D}\tilde{\boldsymbol{\varepsilon}}_{k,i}\,d\Omega-\frac{1}{2}\alpha\underbrace{\int_{\Omega_{k,i}}\tilde{\boldsymbol{\varepsilon}}^T_{k,i}\mathbf{D}\boldsymbol{\varepsilon}^{ad}_{k,i}\,d\Omega}_{=0}-\frac{1}{2}\alpha\underbrace{\int_{\Omega_{k,i}}(\boldsymbol{\varepsilon}^{ad}_{k,i})^T\mathbf{D}\tilde{\boldsymbol{\varepsilon}}_{k,i}\,d\Omega}_{=0}-\frac{1}{2}\alpha^2\int_{\Omega_{k,i}}(\boldsymbol{\varepsilon}^{ad}_{k,i})^T\mathbf{D}\boldsymbol{\varepsilon}^{ad}_{k,i}\,d\Omega\\
&\quad+\int_{\Omega_{k,i}}\tilde{\boldsymbol{\varepsilon}}^T_{k,i}\mathbf{D}\tilde{\boldsymbol{\varepsilon}}_{k,i}\,d\Omega+\alpha\underbrace{\int_{\Omega_{k,i}}(\boldsymbol{\varepsilon}^{ad}_{k,i})^T\mathbf{D}\tilde{\boldsymbol{\varepsilon}}_{k,i}\,d\Omega}_{=0}\\
&= \frac{1}{2}\int_{\Omega_{k,i}}\tilde{\boldsymbol{\varepsilon}}^T_{k,i}\mathbf{D}\tilde{\boldsymbol{\varepsilon}}_{k,i}\,d\Omega-\frac{1}{2}\alpha^2\int_{\Omega_{k,i}}(\boldsymbol{\varepsilon}^{ad}_{k,i})^T\mathbf{D}\boldsymbol{\varepsilon}^{ad}_{k,i}\,d\Omega \qquad (20)\end{aligned}$$

Here due to the zero-sum property by Eq. (12), three terms of integrals vanish. Hence Hellinger–Reissner variational principle is reduced to

$$\Pi_{HR}(\hat{\mathbf{u}},\boldsymbol{\varepsilon}^{ad},\alpha)=\sum_{k=1}^{N}\sum_{i=1}^{M}\left[\frac{1}{2}\int_{\Omega_{k,i}}\tilde{\boldsymbol{\varepsilon}}^T_{k,i}\mathbf{D}\tilde{\boldsymbol{\varepsilon}}_{k,i}\,d\Omega-\frac{1}{2}\alpha^2\int_{\Omega_{k,i}}(\boldsymbol{\varepsilon}^{ad}_{k,i})^T\mathbf{D}\boldsymbol{\varepsilon}^{ad}_{k,i}\,d\Omega\right]-\int_{\Omega}\hat{\mathbf{u}}^T\mathbf{b}\,d\Omega-\int_{\Gamma_t}\hat{\mathbf{u}}^T\bar{\mathbf{t}}\,d\Gamma \qquad (21)$$

which will leads to a symmetric stiffness matrix.

Performing variation corresponding to α, one has

$$\delta_\alpha\Pi_{HR}(\hat{\mathbf{u}},\boldsymbol{\varepsilon}^{ad},\alpha)=-\alpha\sum_{k=1}^{N}\sum_{i=1}^{M}\int_{\Omega_{k,i}}(\boldsymbol{\varepsilon}^{ad}_{k,i})^T\mathbf{D}\boldsymbol{\varepsilon}^{ad}_{k,i}\,d\Omega\Rightarrow\alpha=0 \qquad (22)$$

In this case, Eq. (21) becomes the total potential energy (Π_{TPE}). This is not surprise, because the modified strain becomes the original compatible strain and the standard FEM is recovered. We now perform variation with respect to ε^{ad} (for any finite α)

$$\delta_{\boldsymbol{\varepsilon}^{ad}}\Pi_{HR}(\mathbf{u},\boldsymbol{\varepsilon}^{ad},\alpha)=-\alpha^2\sum_{k=1}^{N}\sum_{i=1}^{M}\int_{\Omega_{k,i}}\mathbf{D}\boldsymbol{\varepsilon}^{ad}_{k,i}\,d\Omega=\mathbf{0}\Rightarrow\int_{\Omega_{k,i}}\boldsymbol{\varepsilon}^{ad}_{k,i}\,d\Omega=\mathbf{0} \qquad (23)$$

which gives the zero-sum Eq. (12).

We next perform variation with respect to $\hat{\mathbf{u}}$ leading to

$$\begin{aligned}\delta_{\hat{\mathbf{u}}}\Pi_{HR}(\hat{\mathbf{u}},\alpha)&=\sum_{k=1}^{N}\sum_{i=1}^{M}\left[\int_{\Omega_{k,i}}\delta\tilde{\boldsymbol{\varepsilon}}^T_{k,i}\mathbf{D}\tilde{\boldsymbol{\varepsilon}}_{k,i}\,d\Omega-\alpha^2\int_{\Omega_{k,i}}(\delta\boldsymbol{\varepsilon}^{ad}_{k,i})^T\mathbf{D}\boldsymbol{\varepsilon}^{ad}_{k,i}\,d\Omega\right]-\int_{\Omega}\delta\mathbf{u}^T\mathbf{b}\,d\Omega-\int_{\Gamma_t}\delta\mathbf{u}^T\bar{\mathbf{t}}\,d\Gamma\\
&=\sum_{k=1}^{N}\sum_{i=1}^{M}\left[\int_{\Omega_{k,i}}\delta(\tilde{\boldsymbol{\varepsilon}}_{k,i}+\alpha\boldsymbol{\varepsilon}^{ad}_{k,i})^T\mathbf{D}(\tilde{\boldsymbol{\varepsilon}}_{k,i}-\alpha\boldsymbol{\varepsilon}^{ad}_{k,i})\mathrm{d}\Omega\right]-\int_{\Omega}\delta\mathbf{u}^T\mathbf{b}\,d\Omega-\int_{\Gamma_t}\delta\mathbf{u}^T\bar{\mathbf{t}}\,d\Gamma=0 \qquad (24)\end{aligned}$$

which is the Galerkin-like weak form given in Eq. (15) that is variational consistent, because it is derived from the Hellinger–Reissner variational principle. □

The new Galerkin-like weakform Eq. (15) is as simple as the Galerkin weak formulation: the bi-linear form is still symmetric, and hence the SαFEM should keep all the good properties of the standard Galerkin weak form. The Galerkin-like weakform provides a "legal" means to re-construct the strain field. In the case of no reconstruction is made, we have $\boldsymbol{\varepsilon}^{ad}_{k,i}=0$, and the Galerkin-like becomes the standard Galerkin weakform.

Substituting the approximation Eq. (1) into Eq. (15) and using the arbitrary property of variation, we obtain

$$\widehat{\mathbf{K}}^{\mathrm{S\alpha FEM}}_{\alpha}\hat{\mathbf{d}}=\hat{\mathbf{f}} \qquad (25)$$

where $\widehat{\mathbf{K}}^{\mathrm{S\alpha FEM}}_{\alpha}$ is the element stiffness matrix with the scaled gradient strains, and $\hat{\mathbf{f}}$ is the element force vector given by

$$\widehat{\mathbf{K}}^{\mathrm{S\alpha FEM}}_{\alpha}=\underbrace{\sum_{k=1}^{N}\sum_{i=1}^{M}\int_{\Omega_{k,i}}\mathbf{B}^T_{k,i}\mathbf{D}\mathbf{B}_{k,i}\,d\Omega}_{\mathbf{K}^{\mathrm{FEM\text{-}T3}}}-\alpha^2\underbrace{\sum_{k=1}^{N}\sum_{i=1}^{M}\int_{\Omega_{k,i}}(\mathbf{B}^{ad}_{k,i})^T\mathbf{D}\mathbf{B}^{ad}_{k,i}\,d\Omega}_{\widehat{\mathbf{K}}_{ad}}=\mathbf{K}^{\mathrm{FEM\text{-}T3}}-\alpha^2\widehat{\mathbf{K}}^{\mathrm{S\alpha FEM}}_{ad} \qquad (26)$$

$$\hat{\mathbf{f}}=\int_{\Omega}\mathbf{N}^T(\mathbf{x})\mathbf{b}\,d\Omega+\int_{\Gamma_{\mathbf{t}}}\mathbf{N}^T(\mathbf{x})\bar{\mathbf{t}}\,d\Gamma \qquad (27)$$

where $\mathbf{K}^{\mathrm{FEM\text{-}T3}}$ is the global stiffness matrix of the standard FEM (T3). $\widehat{\mathbf{K}}^{\mathrm{S\alpha FEM}}_{ad}$ is derived from the correction strain, and hence it is termed as correction stiffness matrix that help to reduce the well-known overly-stiffness of the standard FEM model. In Eq. (26),

$$\mathbf{B}^{ad}_{k,i}=\sqrt{6}(\bar{\mathbf{B}}_k-\mathbf{B}_{k,i})\left(L_1-\frac{1}{3}\right) \qquad (28)$$

and $\widehat{\mathbf{K}}_{ad}^{\mathrm{S\alpha FEM}}$ can be rewritten explicitly as

$$\begin{aligned}\widehat{\mathbf{K}}_{ad}^{\mathrm{S\alpha FEM}} &= \sum_{k=1}^{N}\sum_{i=1}^{M}\int_{\Omega_{k,i}}(\mathbf{B}_{k,i}^{ad})^T\mathbf{D}\mathbf{B}_{k,i}^{ad}\,d\Omega = 6\sum_{k=1}^{N}\sum_{i=1}^{M}(\overline{\mathbf{B}}_k-\mathbf{B}_{k,i})^T\mathbf{D}(\overline{\mathbf{B}}_k-\mathbf{B}_{k,i})\int_{\Omega_{k,i}}\left(L_1-\frac{1}{3}\right)^2 d\Omega \\ &= \frac{1}{3}\sum_{k=1}^{N}\sum_{i=1}^{M}(\overline{\mathbf{B}}_k-\mathbf{B}_{k,i})^T\mathbf{D}(\overline{\mathbf{B}}_k-\mathbf{B}_{k,i})A_{k,i}\end{aligned} \tag{29}$$

where $\overline{\mathbf{B}}_k = \frac{1}{A_k}\sum_{i=1}^{M}\int_{\Omega_{k,i}}\mathbf{B}_{k,i}\,d\Omega = \frac{1}{A_k}\sum_{i=1}^{M}A_{k,i}\mathbf{B}_{k,i}$ is the nodal strain displacement matrix of node k, $\mathbf{B}_{k,i}$ is the strain displacement matrix of sub-triangular domain i connecting to vertex k, e.g. Fig. 2.

It is clear that correction stiffness matrix $\widehat{\mathbf{K}}_{ad}^{\mathrm{S\alpha FEM}}$ counts for the *strain gap* (cf. Eq. (10)) between the compatible (element) strains of FEM and the smoothed nodal strains of the NS-FEM. Note that the present formulation (cf. Eq. (26)) is always stable for any finite parameters α. Hence α can be manipulated without affecting the convergence of the model [51], and it plays a crucial role to ensure the accuracy of the model. Manipulating $\widehat{\mathbf{K}}_{ad}^{\mathrm{S\alpha FEM}}$ through α can, however, change the convergent *rate* of the model.

Eq. (26) may be rewritten in the following form:

$$\underbrace{\widehat{\mathbf{K}}_{\alpha}^{\mathrm{S\alpha FEM}}}_{\mathrm{SPD}} = \underbrace{\widehat{\mathbf{K}}_{\alpha=0}^{\mathrm{S\alpha FEM}}}_{\mathbf{K}^{\mathrm{FEM\text{-}T3}},\mathrm{SPD}} - \alpha^2\underbrace{\widehat{\mathbf{K}}_{ad}^{\mathrm{S\alpha FEM}}}_{\mathrm{SPD}} \tag{30}$$

Here we note the symmetric positive definite (SPD) property of all these matrices after the imposition of the essential boundary condition for a well-posed problem.

4. Properties of the SαFEM model

Remark 1 (*Variational consistence*). The present method is variationally consistent for any real finite α, because it is derived from the modified Hellinger–Reissner principle rooted from the Hu–Washizu principle.

Owing to the SPD property of $\widehat{\mathbf{K}}_{\alpha}^{\mathrm{S\alpha FEM}}$, $\widehat{\mathbf{K}}_{\alpha=0}^{\mathrm{S\alpha FEM}}$ (or $\mathbf{K}^{\mathrm{FEM\text{-}T3}}$) and $\widehat{\mathbf{K}}_{ad}^{\mathrm{S\alpha FEM}}$, Eq. (26) shows clearly that $\widehat{\mathbf{K}}_{\alpha}^{\mathrm{S\alpha FEM}}$ is "softer" than $\mathbf{K}^{\mathrm{FEM\text{-}T3}}$. In other words, the scaling of the strain gap by factor α creates a "softer" model. We next state

Remark 2 (*Softening effect*). The scaling to the strain gap always provides softening effects. This means that the present model is "softer" than the fully-compatible FEM-T3 model for any scaling finite real factor α.

Remark 3 (*Existence of critical* α). From Eq. (26), it is clear that for a finite mesh, $\widehat{\mathbf{K}}_{\alpha}^{\mathrm{S\alpha FEM}}$ can even be made negative definite for a sufficiently large parameter α. Therefore, there exists a smallest α such that $\widehat{\mathbf{K}}_{\alpha}^{\mathrm{S\alpha FEM}}$ is SPD. The smallest α is termed as the critical α or α_{cr}. The critical α can be found as the smallest eigenvalue of the following eigenvalue problem:

$$\left[\widehat{\mathbf{K}}_{\alpha=0}^{\mathrm{S\alpha FEM}} - \alpha_{cr}^2\widehat{\mathbf{K}}_{ad}^{\mathrm{S\alpha FEM}}\right]\mathbf{\Phi} = \mathbf{0} \tag{31}$$

The SPD property of $\widehat{\mathbf{K}}_{\alpha=0}^{\mathrm{S\alpha FEM}}$ and $\widehat{\mathbf{K}}_{ad}^{\mathrm{S\alpha FEM}}$ ensures a unique solution to the above eigenvalue equation, and hence an α_{cr} can always be found.

Note that at α_{cr}, the solution can become infinite. This implies that the present model can be made to be as soft as possible by using an α that approaches to α_{cr}. This property is useful, because it ensures that the present model can be made to be "soft" enough to give an upper bound to the exact solution of any well-posed problems.

Note also that in practical application of present method, there is no need to solve the expensive eigenvalue problem defined in Eq. (31). The eigenvalue argument used here is only of theoretical importance, because the existence of α_{cr} is needed to prove important properties of the present method.

Remark 4 (*SPD*). When $0 \leqslant \alpha < \alpha_{cr}$, the stiffness matrix $\widehat{\mathbf{K}}_{\alpha}^{\mathrm{S\alpha FEM}}$ is an even parabolic function of α. It varies continuously from $\widehat{\mathbf{K}}_{\alpha=0}^{\mathrm{S\alpha FEM}}$ to $\widehat{\mathbf{K}}_{\alpha=0}^{\mathrm{S\alpha FEM}} - \alpha_{cr}^2\widehat{\mathbf{K}}_{ad}^{\mathrm{S\alpha FEM}}$. It is SPD for well-posed problems, because of Remark 3.

Remark 5 (*Bottom-line: proven fact*). When $\alpha = 0.0$, we have $\widehat{\mathbf{K}}_{(\alpha=0)}^{S\alpha FEM} = \mathbf{K}^{\mathrm{FEM\text{-}T3}}$. The present method becomes the standard FEM-T3.

We now prove the fact that the solution of the present model will converge, as long as the original problem is well-posed.

Property 2 (Convergence property). *For any given finite real number $0 \leqslant \alpha < \alpha_{cr}$, the SαFEM solution always converges to the exact solution when the dimensions of all the smoothing cells approach to zero.*

Proof. Eq. (17) can be rewritten as

$$\widehat{\mathbf{U}}(\alpha) = \frac{1}{2}\sum_{k=1}^{N}\sum_{i=1}^{M}\int_{\Omega_{k,i}} \tilde{\boldsymbol{\varepsilon}}_{k,i}^{T}\mathbf{D}\tilde{\boldsymbol{\varepsilon}}_{k,i}\,d\Omega - \alpha^2\frac{1}{2}\sum_{k=1}^{N}\sum_{i=1}^{M}\int_{\Omega_{k,i}} (\boldsymbol{\varepsilon}_{k,i}^{ad})^{T}\mathbf{D}\boldsymbol{\varepsilon}_{k,i}^{ad}\,d\Omega$$
$$= \frac{1}{2}\sum_{k=1}^{N}\sum_{i=1}^{M}\int_{\Omega_{k,i}} \tilde{\boldsymbol{\varepsilon}}_{k,i}^{T}\mathbf{D}\tilde{\boldsymbol{\varepsilon}}_{k,i}\,d\Omega - \alpha^2\frac{1}{2}\sum_{k=1}^{N}\sum_{i=1}^{M}\int_{\Omega_{k,i}} (\bar{\boldsymbol{\varepsilon}}_{k} - \tilde{\boldsymbol{\varepsilon}}_{k,i})^{T}\mathbf{D}(\bar{\boldsymbol{\varepsilon}}_{k} - \tilde{\boldsymbol{\varepsilon}}_{k,i})d\Omega \tag{32}$$

From the definition of smoothed strain $\bar{\boldsymbol{\varepsilon}}_k$, the nodal smoothed strains will approach to the compatible strain $\tilde{\boldsymbol{\varepsilon}}(\tilde{\boldsymbol{\varepsilon}}_{k,i} = \lim_{A_{k,i}\to 0}\bar{\boldsymbol{\varepsilon}}_k = \lim_{A_{k,i}\to 0}\frac{1}{A_{k,i}}\int_{\Omega_{k,i}}\nabla_s\widehat{\mathbf{u}}\,d\Omega)$ when the size of all smoothing cells approaches zero. Therefore, one has

$$\sum_{k=1}^{N}\sum_{i=1}^{M}\int_{\Omega_{k,i}} (\bar{\boldsymbol{\varepsilon}}_{k} - \tilde{\boldsymbol{\varepsilon}}_{k,i})^{T}\mathbf{D}(\bar{\boldsymbol{\varepsilon}}_{k} - \tilde{\boldsymbol{\varepsilon}}_{k,i})d\Omega \to 0 \tag{33}$$

At this limit, Eq. (32) becomes the standard FEM formulation that has been proven to converge to the exact solution. Thus, this completes the proof of Property 2. □

This property ensures that the present solution will converge with any finite real number $0 \leqslant \alpha < \alpha_{cr}$. However, the convergence rate and bound properties are effected by the choice of α. An ideal α can give the exact solution in energy norm, but it can be expensive to find. A preferred α can be quite easily and less expensively found to produce a superconvergent solution, or "tight" solution bounds. This is stated in the following theorem.

Property 3 (Bounds to the exact solution). *There exists an $\alpha_{upper} \in [0, \alpha_{cr})$, such that the exact solution in energy norm is bounded by*

$$\widehat{U}(\alpha = 0) \leqslant U_{exact} \leqslant \widehat{U}(\alpha_{upper}) \tag{34}$$

Proof. First, by definition we immediately have

$$\widehat{U}(\alpha = 0) \leqslant U_{exact} \tag{35}$$

From Eq. (26) and for any admissible $\tilde{\mathbf{d}}$, we have

$$\underbrace{\tilde{\mathbf{d}}^{T}\widehat{\mathbf{K}}_{\alpha}^{S\alpha FEM}\tilde{\mathbf{d}}}_{>0} = \underbrace{\tilde{\mathbf{d}}^{T}\mathbf{K}^{FEM}\tilde{\mathbf{d}}}_{>0} - \alpha^2\underbrace{\tilde{\mathbf{d}}^{T}\widehat{\mathbf{K}}_{ad}^{S\alpha FEM}\tilde{\mathbf{d}}}_{>0}, \quad \forall\alpha \in [0, \alpha_{cr}) \tag{36}$$

which means that

$$\tilde{\mathbf{d}}^{T}\widehat{\mathbf{K}}_{\alpha}^{S\alpha FEM}\tilde{\mathbf{d}} \leqslant \tilde{\mathbf{d}}^{T}\widehat{\mathbf{K}}^{FEM}\tilde{\mathbf{d}}, \quad \forall\alpha \in [0, \alpha_{cr}) \tag{37}$$

which implies that [40]

$$\widehat{U}_{\alpha}^{S\alpha FEM} \geqslant \widehat{U}_{\alpha=0}^{S\alpha FEM} = U^{FEM}, \quad \forall\alpha \in [0, \alpha_{cr}) \tag{38}$$

Eq. (37) shows that the stiffness matrix of the SαFEM is "*softer*" than that of the FEM-T3 element.

On the other hand, from Remark 2 we can make the SαFEM as soft as possible by increasing α. To show this mathematically, we consider a well-posed problem in which the solution in displacement $\hat{\mathbf{d}}$ obtained using the SαFEM model can be expressed as

$$\hat{\mathbf{d}} = \sum_{i}^{N_{dof}} c_i\boldsymbol{\Phi}_i \tag{39}$$

where $\boldsymbol{\Phi}_i$ is the ith eigenvector obtained by solving Eq. (31), c_i is the ith model participation factor that can be determined by substituting Eq. (39) into Eq. (26), and N_{dof} is the number of the total unconstrained degree of freedom of the model. Using Eqs. (36) and (39), and the orthogonal properties of these eigenvectors, we have

$$\alpha^2\sum_{i}^{N_{dof}} c_i\boldsymbol{\Phi}_i^{T}\widehat{\mathbf{K}}_{ad}^{S\alpha FEM}\boldsymbol{\Phi}_i^{T} = \sum_{i}^{N_{dof}} c_i\boldsymbol{\Phi}_i^{T}\widehat{\mathbf{K}}_{\alpha=0}^{S\alpha FEM}\boldsymbol{\Phi}_i^{T} - \sum_{i}^{N_{dof}} c_i\boldsymbol{\Phi}_i^{T}\widehat{\mathbf{K}}_{\alpha}^{S\alpha FEM}\boldsymbol{\Phi}_i \tag{40}$$

For the well-posed problem, there exists an exact solution with strain energy $U_{\text{exact}} > 0$. To obtain an upper bound solution in energy by using the SαFEM model, we need

$$\hat{\mathbf{d}}^{T}\widehat{\mathbf{K}}_{\alpha_{upper}}^{S\alpha FEM}\hat{\mathbf{d}} = \sum_{i}^{N_{dof}} c_i\boldsymbol{\Phi}_i^{T}\widehat{\mathbf{K}}_{\alpha_{upper}}^{S\alpha FEM}\boldsymbol{\Phi}_i \geqslant U_{exact} \tag{41}$$

Substituting Eq. (41) into (40), we now find

$$\alpha_{upper}^2 \leqslant \frac{\sum_i^{N_{dof}} c_i\boldsymbol{\Phi}_i^{T}\widehat{\mathbf{K}}_{\alpha=0}^{S\alpha FEM}\boldsymbol{\Phi}_i^{T} - U_{exact}}{\sum_i^{N_{dof}} c_i\boldsymbol{\Phi}_i^{T}\widehat{\mathbf{K}}_{ad}^{S\alpha FEM}\boldsymbol{\Phi}_i^{T}} \leqslant \alpha_{cr}^2 \tag{42}$$

Using the α_{upper} satisfying Eq. (42), we have

$$U_{exact} \leqslant \widehat{U}(\alpha_{upper}) \tag{43}$$

The combination of Eqs. (35) and (43) gives (34). □

This proof using the eigenvalue argument shows theoretically the existence of α_{upper} and the fact that the SαFEM can always produce upper bounds. Our numerical experience has shown that for given problems, an α_{upper} usually exists. In addition, the exact value of α_{upper} is not important. Any α_{upper} of which strain energy is reasonably close to the exact energy can create an upper bound. Therefore, in practical application of the SαFEM, there is no need to solve the expensive eigenvalue problem defined by Eq. (31). Our numerical experience shows that α_{upper} may be simply fixed at 1.7 and it works well for all numerical examples tested.

Remark 6 (*Negative* α). It is observed that $\widehat{U}(\alpha)$ is an even function of second order of the scaling factor α. Therefore, the present method also converges for any negative real finite $-\alpha_{cr} < \alpha \leqslant 0$ when the mesh size tends to zero.

5. Free of volumetric locking: a combined SαFEM/NS-FEM model

Similar to the standard FEM, the SαFEM can lead to a poor accuracy for plane strain problems in the nearly incompressible limit. This is well-known as volumetric (or Poisson's) locking. One of the ways to overcome this problem is to use selective formulations in the conventional FEM [1]. In this work, we use selectively two different models for two different material "terms" (deviatoric term and volumetric term). The SαFEM is applied to the deviatoric term, while the NS-FEM [39] which was demonstrated effectively to overcome the volumetric locking is applied to the volumetric term. The details are given below

The material property matrix **D** for isotropic materials is first rewritten as

$$\mathbf{D} = \mathbf{D}_{dev} + \mathbf{D}_{vol} \tag{44}$$

where $\mathbf{D}_{dev}$, $\mathbf{D}_{vol}$ are deviatoric and volumetric matrices, respectively

$$\mathbf{D}_{dev} = \mu \begin{bmatrix} 2 & 0 & 0 \\ 0 & 2 & 0 \\ 0 & 0 & 1 \end{bmatrix}, \quad \mathbf{D}_{vol} = \lambda \begin{bmatrix} 1 & 1 & 0 \\ 1 & 1 & 0 \\ 0 & 0 & 0 \end{bmatrix} \tag{45}$$

where the shearing modulus $\mu = E/2(1+\nu)$, and the Lame's parameter $\lambda = 2\nu\mu/(1-2\nu)$.

In our model-based selective scheme, we use the SαFEM to calculate the stiffness matrix related to the deviatoric term and the NS-FEM to calculate the one related to the volumetric term. Therefore, the stiffness matrix of the combined Sα/NS-FEM model becomes

$$\widehat{\mathbf{K}} = \widehat{\mathbf{K}}_{\alpha}^{\text{S}\alpha\text{FEM}} + \widehat{\mathbf{K}}^{\text{NS-FEM}} \tag{46}$$

where $\widehat{\mathbf{K}}_{\alpha}^{\text{S}\alpha\text{FEM}}$ is given by Eq. (26), and

$$\widehat{\mathbf{K}}^{\text{NS-FEM}} = \sum_{k=1}^{N} \sum_{i=1}^{M} \int_{\Omega_{k,i}} \overline{\mathbf{B}}_k^T \mathbf{D}_{vol} \overline{\mathbf{B}}_k \, d\Omega \tag{47}$$

By this way, the present method is free of volumetric locking for any finite value α when the Poisson's ratio approaches to 0.5. An interesting point here is that our method can deal with nearly incompressible cases without using additional degrees of freedom as presented in [6,8–10]. Therefore, our formulation provides an alternative and simple way to solve volumetric locking problems. It works as long as the splitting of **D** in Eq. (44) can be performed.

6. Numerical implementation

The numerical procedure for the present SαFEM can be briefed as follows:

1. Discrete the domain Ω into two sets of mesh including one coarse mesh and one finer mesh with the same aspect ratio ($M^{(1)}$, $M^{(2)}$) [50,51] of triangular elements such that $\Omega = \sum_{i=1}^{nel} \Omega^i$ and $\Omega^i \cap \Omega^j = \emptyset, i \neq j$;
2. Create smoothing domains Ω_k such that $\Omega = \sum_{k=1}^{N_n} \Omega_k$ and $\Omega_i \cap \Omega_j = \emptyset$, $i \neq j$.
3. Choose one array of $\alpha \in [1.3, 1.7]$, for instance $\alpha \in [1.3 \quad 1.4 \quad 1.5 \quad 1.6 \quad 1.7]$.
4. Loop over each set of meshes generated in step 1

    {

    • Loop over a set $\alpha \in [1.3, 1.7]$

    {

    ○ Loop over all nodes

    {

+ Compute the area of smoothing domains Ω_k associated with nodes k and find neighbouring smoothing domains of each node.
+ Evaluate the gradient matrix $\overline{\mathbf{B}}_k, \mathbf{B}_{k,i}$ in Eqs. (26), (28).
+ Compute the stiffness matrices $\mathbf{K}^{\text{FEM-T3}}, \widehat{\mathbf{K}}_{ad}^{\text{S}\alpha\text{FEM}}$ and $\mathbf{K}^{\text{FEM-T3}} - \alpha^2 \widehat{\mathbf{K}}_{ad}^{\text{S}\alpha\text{FEM}}$ in Eq. (26) and load vector in the current smoothing domain.
+ Assemble the stiffness matrix and force vector of current smoothing domain into the global stiffness matrix and load vector.

}// End the loop over all nodes

- Apply boundary conditions
- Solve system equations to determinate nodal displacements
- Compute strain energy against each value α and store all energies $\widehat{U}^{(i)}(\alpha)$ into an array, for example,

$$\forall i = 1,2 : E^{(i)} = \left[\widehat{U}^{(i)}(1.3)\ \widehat{U}^{(i)}(1.4)\ \widehat{U}^{(i)}(1.5)\ \widehat{U}(1.6)\ \widehat{U}^{(i)}(1.7)\right]$$

}// End the loop over the array $\alpha \in [1.3, 1.7]$

}// End the loop over two sets of given meshes

5. Interpolate and evaluate the intersection point $\alpha^{(12)}$ from two curves $E^{(1)}$, $E^{(2)}$.
6. Repeat steps from 1 to 5 for two sets of successively finer meshes (h_i, $i = 2,3$) with the same aspect ratio and calculate the intersection point $\alpha^{(23)}$ from two curves $E^{(2)}$, $E^{(3)}$.

It is observed from numerical results that when an $\alpha \in$ [1.3, 1.7] is used directly for any meshes, SαFEM solutions are always much better than those of FEM-T3, FEM-Q4, NS-FEM-T3, and even much better than ES-FEM-T3 [45] that has been found to be one of the most accurate models using triangular meshes.

I0f we want to reproduce sufficiently both upper and lower bounds of solution, an $\alpha \in [1.3, 1.7]$ can be also found. In addition, we can show the superconvergent property of the model in the energy error norm for solid mechanics problems via the effective manipulation of α-parameter.

7. Determination of preferable α for superconvergent solution

As demonstrated in Section 8, the SαFEM can produce "exact" solutions or a superconvergent solution for both displacement and energy norms by properly choosing the scaling factor α. Therefore a question now is that how to find such an "exact" value α. Our numerical tests show that α_{exact} is not only problem-dependent but also mesh-dependent [50–52]. In this work we only concern on the superconvergent property in the energy norm, and hence a "preferable" α needs to be chosen to achieve such a solution. We adopt the procedure proposed in [55] to find such "preferable" α, and assume

$$\alpha_{pref}(h) = ah + b \tag{48}$$

where a and b are unknown and problem-dependent constants, which can be determined from the intersection $\alpha^{(12)}$ and $\alpha^{(23)}$ obtained in Section 6. Hence, Eq. (48) becomes

$$\alpha_{exact}(h) \approx \alpha_{pref}(h) = \frac{\alpha^{(12)}(h_1) - \alpha^{(23)}(h_2)}{h_1 - h_2}(h - h_1) + \alpha^{(12)}(h_1) \tag{49}$$

where h_1, $h_2$are the average nodal spacing of two sets of meshes ($M^{(1)}$, $M^{(2)}$) and ($M^{(2)}$, $M^{(3)}$), respectively.

Eq. (49) provides a simple way to find a preferable α that can lead to the superconvergent solution in the energy norm.

8. Numerical study

In this section, benchmark problems are examined using the SαFEM. For comparison, the following models are used.

- T3 – three-node element of the standard FEM with shape linear function.
- Q4 – 4-node quadrilateral element the standard FEM using 2×2 Gauss points.
- EQ4 – 4-node quadrilateral element of the equilibrium model [66].
- NS-T3 – the nodal-based SFEM using triangular meshes (NS-FEM-T3) [39].
- ES-T3 – the edge-based SFEM (ES-FEM-T3) [45] that was found to be one of the "most" accurate models using linear triangular elements.

8.1. Standard patch test: linear reproducibility/convergence

In order to check numerically the convergence of the present SαFEM stated theoretically by Property 2, the standard patch test [67] is first conducted. The patch used in the test is shown in Fig. 3. The exact displacement, strain and stress are given by

$$u = 10^{-3}(x + y/2), \quad v = 10^{-3}(x/2 + y)$$
$$\varepsilon_x = \varepsilon_x = \gamma_{xy} = 10^{-3}, \quad \sigma_x = \sigma_y = 1333, \quad \tau_{xy} = 400 \tag{50}$$

Our numerical tests have found that the exact values are reproduced to machine precision. Hence, the present SαFEM for any finite α passes the standard patch test.

8.2. Cantilever beam loaded at the end: convergence study and volumetric locking

In order to examine the numerical convergence rate of the present method, two norms are used: displacement error norm and energy error norm. The displacement error norm is defined as

$$e_d = \frac{\sum_{i=1}^{ndof} |u_i - u_i^h|}{\sum_{i=1}^{ndof} |u_i|} \times 100\% \tag{51}$$

where u_i is the exact and u_i^h is the numerical solution of the displacements. The energy error norm is defined by

$$e_e(\alpha) = |\widehat{U}(\alpha) - U_{exact}|^{1/2} \tag{52}$$

where the total strain energy of numerical solution $E(\alpha)$

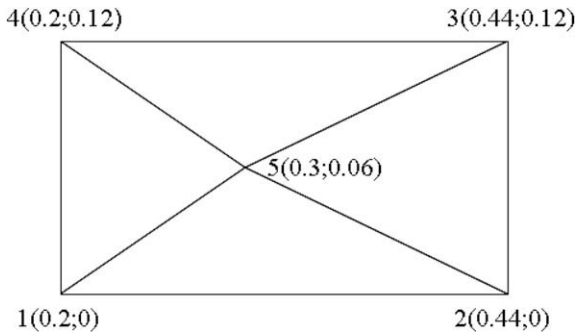

Fig. 3. Constant strain/stress patch test ($E = 10^6$, $\nu = 0.25$, thickness $t = 0.001$).

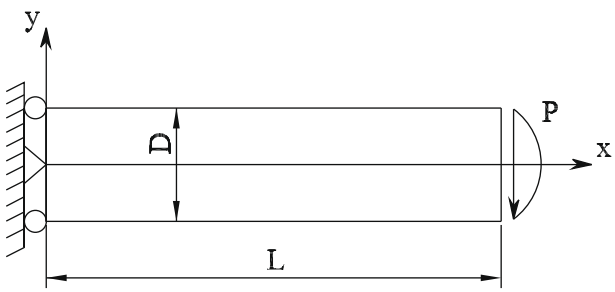

Fig. 4. A rectangular cantilever and boundary conditions of a cantilever subjected to a parabolic traction at the free end.

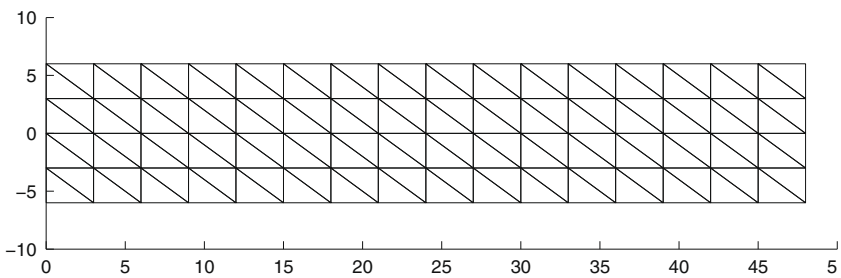

Fig. 5. Domain discretization using 64 rectangular (or 128 triangular) elements of the cantilever beam.

$$\widehat{U}(\alpha) = \frac{1}{2}\hat{\mathbf{d}}^T\widehat{\mathbf{K}}\hat{\mathbf{d}} = \frac{1}{2}\hat{\mathbf{d}}^T\left\{\sum_{k=1}^{N}\sum_{i=1}^{M}\int_{\Omega_{k,i}}\mathbf{B}_{k,i}^T\mathbf{D}\mathbf{B}_{k,i}\,d\Omega - \alpha^2\sum_{k=1}^{N}\sum_{i=1}^{M}\int_{\Omega_{k,i}}(\mathbf{B}_{k,i}^{ad})^T\mathbf{D}\mathbf{B}_{k,i}^{ad}\,d\Omega\right\}\hat{\mathbf{d}} \tag{53}$$

and U_{exact} is the exact strain energy of the problem.

A rectangular cantilever with length L and height D and a unit thickness is studied as a benchmark here, which is subjected to a parabolic traction at the free end as shown in Fig. 4. The analytical solution is available and can be found in a textbook by Timoshenko and Goodier [68].

$$\begin{aligned} u_x &= \frac{Py}{6\bar{E}I}\left[(6L-3x)x + (2+\bar{\nu})(y^2 - \frac{D^2}{4})\right] \\ u_y &= -\frac{P}{6\bar{E}I}\left[3\bar{\nu}y^2(L-x) + (4+5\bar{\nu})\frac{D^2x}{4} + (3L-x)x^2\right] \end{aligned} \tag{54}$$

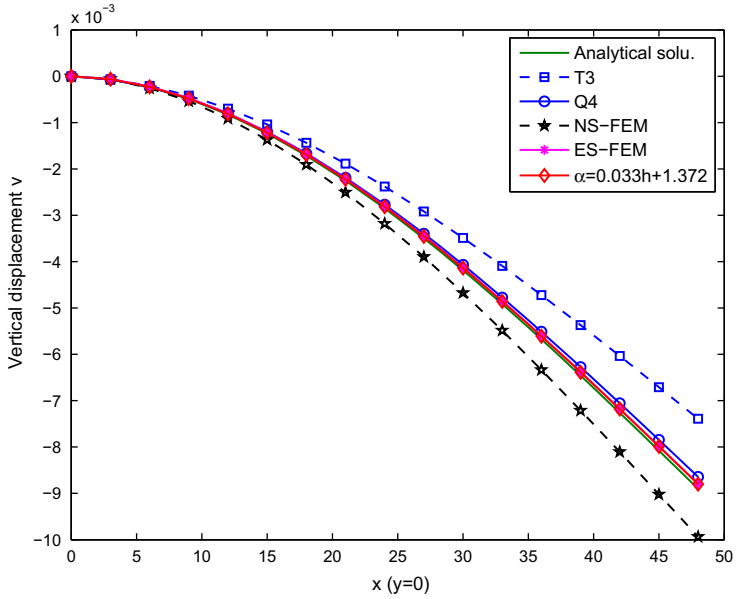

Fig. 6. Vertical displacement at central line ($y = 0$) using 128 triangular elements of the cantilever beam with $\alpha_{pref}(h) = 0.033h + 1.372$.

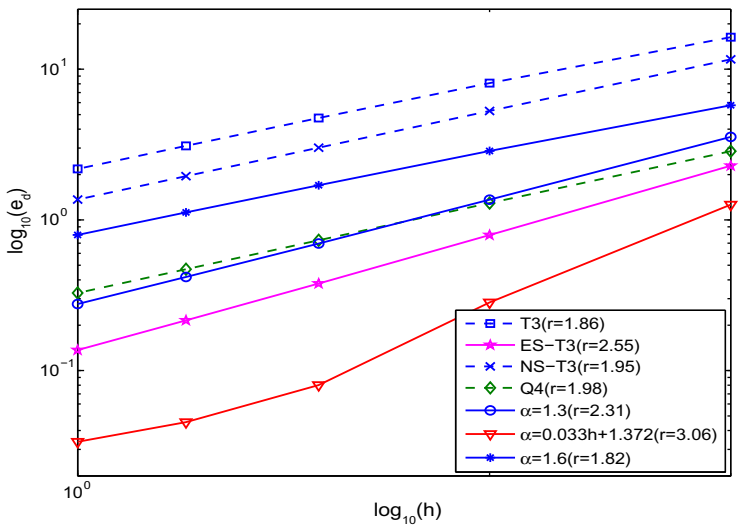

Fig. 7. Convergence and the estimated rate in the displacement norm of the cantilever beam.

where the moment of inertia I for a beam with rectangular cross section and unit thickness is given by $I = \frac{D^3}{12}$ and

$$\bar{E} = \begin{cases} E \\ E/(1-\nu^2) \end{cases}, \quad \bar{\nu} = \begin{cases} \nu & \text{for plan stress} \\ \nu/(1-\nu) & \text{for plan strain} \end{cases} \tag{55}$$

The stresses corresponding to the displacements Eq. (54) are

$$\sigma_{xx}(x,y) = \frac{P(L-x)y}{I}; \quad \sigma_{yy}(x,y) = 0; \quad \tau_{xy}(x,y) = -\frac{P}{2I}\left(\frac{D^2}{4} - y^2\right) \tag{56}$$

The related parameters are taken as $E = 3.0 \times 10^7$ kPa, $D = 12$ m, $L = 48$ m and $P = 1000$ N.

Discretization with 128 triangular elements is illustrated in Fig. 5. Under plane stress conditions and Poisson ratio $\nu = 0.3$, Fig. 6 plots the displacements along the neutral axis. The result shows that the SαFEM produces very good results compared

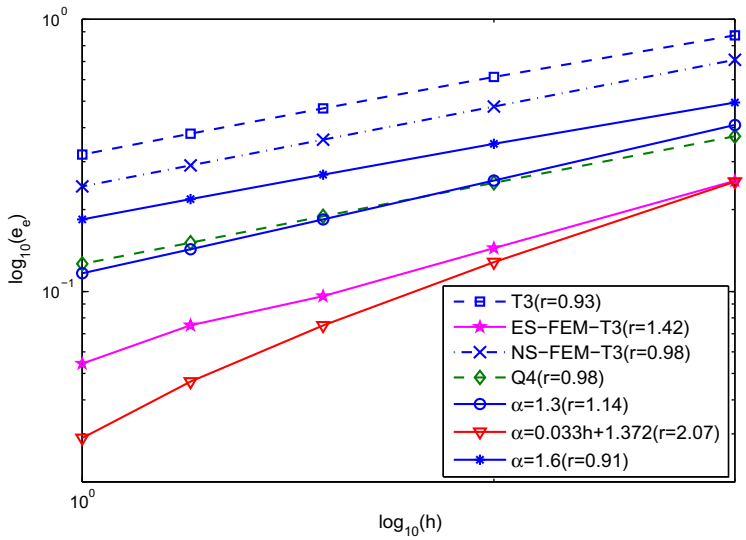

Fig. 8. Convergence and the estimated rate in the energy norm of the cantilever beam.

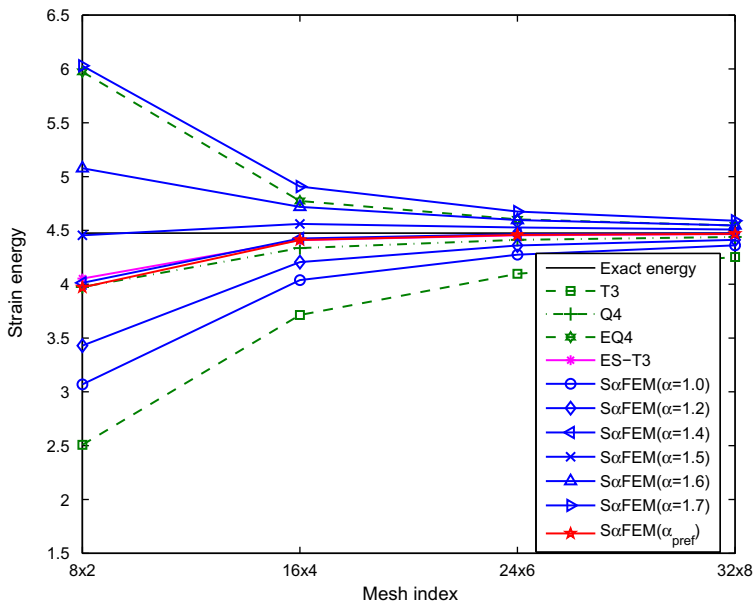

Fig. 9. Solution bounds of energy for the cantilever beam.

to those of others elements. Here we use the procedure given in Section 7 to compute α_{pref} which is found to be $\alpha_{pref}(h) = 0.033h + 1.372$.

Next we plot the convergence rates of the displacement and energy error norms using $\alpha_{pref}(h) = 0.033h + 1.372$ and two other α values. Fig. 7 shows the convergence rate in the displacement norm. The results of the present method are compared to those of T3, Q4, NS-T3 and ES-T3. It is observed that the SαFEM with $\alpha_{pref}(h)$ is superconvergent in displacement norm. It is well-known that the theoretical convergence rate in displacement norm for linear FEM is 2.0, and the numerical rate for T3 is 1.86 slightly below the theoretical rate. The ES-T3 achieved 2.55 that is far above the theoretical value, and the present SαFEM with $\alpha_{pref}(h)$ achieved 3.06 which is even better than the ES-FEM. The present SαFEM can achieve the superconvergent rate for the displacement error norm for this problem, which is clearly different from the usual concept of superconvergence property only in the energy norm in the standard FEM. In terms of accuracy, the SαFEM with $\alpha_{pref}(h)$ clearly stands out and is about 20 times more accurate than the T3, and even 7 times more accurate than Q4. The SαFEM with $\alpha_{pref}(h)$ is also much more (about 4 times) accurate than the ES-T3. Note that the SαFEM with $\alpha = 1.3$ performed as well as the Q4.

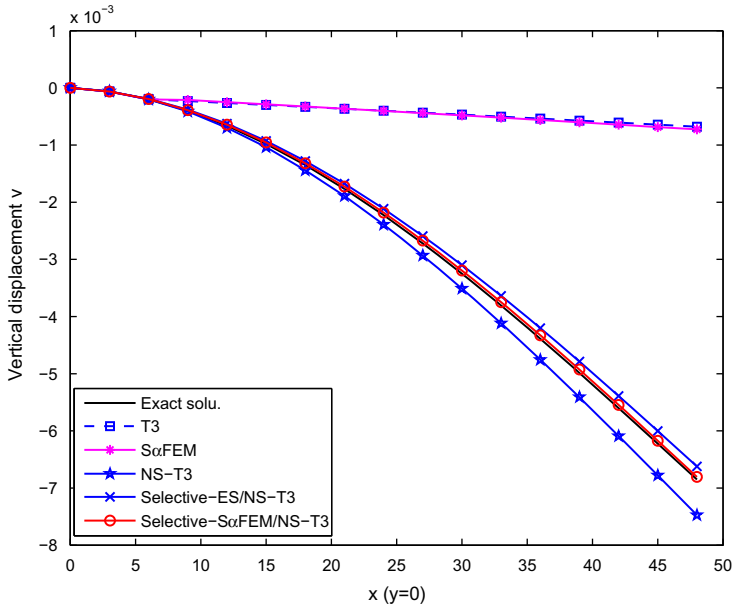

Fig. 10. Vertical displacement for the cantilever beam at the nodes along the x-axis (y=0) using the node-based selective technique with $\nu = 0.4999$.

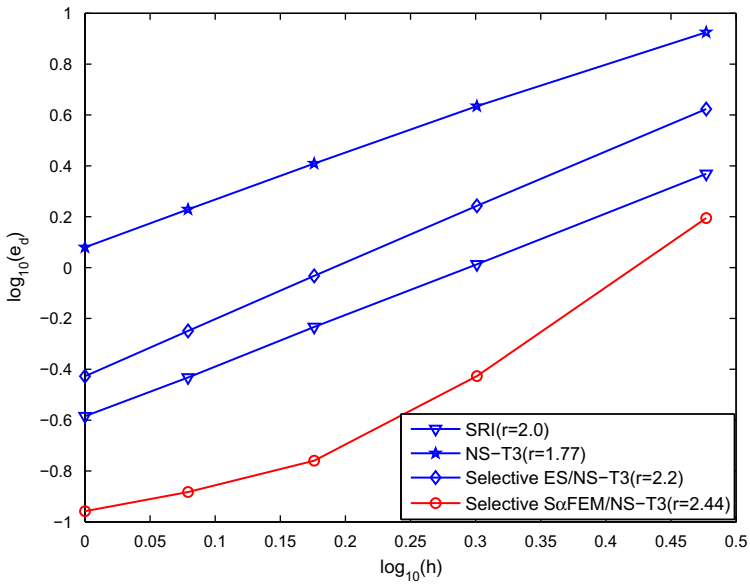

Fig. 11. Convergence of some "looking free" models in the displacement error for the cantilever beam ($\nu = 0.4999$).

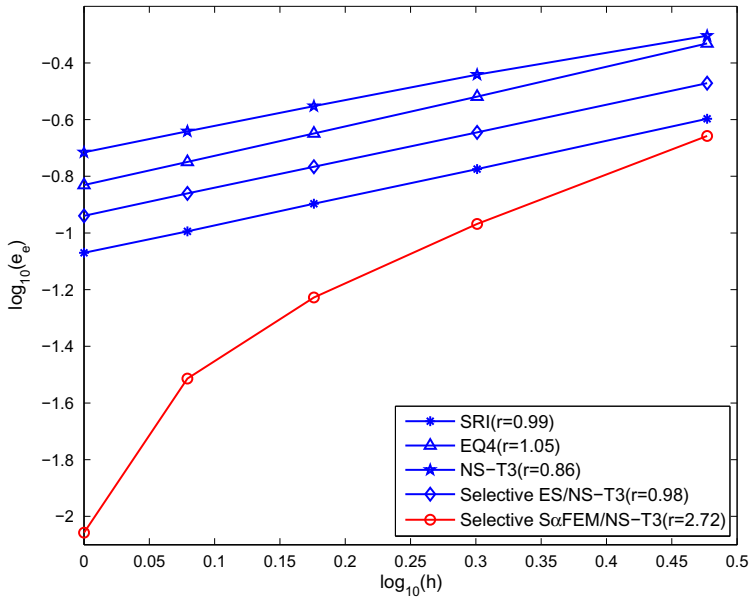

Fig. 12. Convergence and the estimated rate of some "looking free" models in the energy error for the cantilever beam ($\nu = 0.4999$).

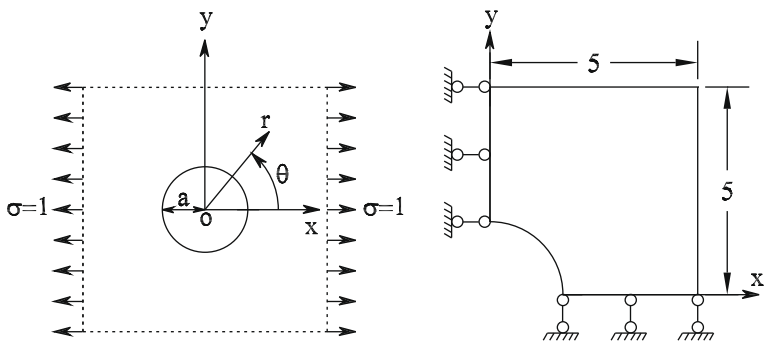

Fig. 13. Infinite plate with a circular hole and its quarter model.

Fig. 8 illustrates the convergence rate in the energy norm. It is observed that the SαFEM with $\alpha_{pref}(h)$ is superconvergent in energy norm. The theoretical convergence rate in energy norm for linear FEM is 1.0, and the numerical rate for FEM-T3 is 0.93 which is slightly below the theoretical rate. The ES-T3 achieved 1.42 that is far above the theoretical value. The present SαFEM with $\alpha_{pref}(h)$ achieved 2.07 that is even better than the ES-FEM. In terms of accuracy, the ES-FEM and the SαFEM with $\alpha_{pref}(h)$ are the best ones which are about 7 times more accurate than the T3, and even about 3 times better than Q4. The SαFEM with $\alpha_{pref}(h)$ is little more (about 1.4 times) accurate than the ES-T3. The SαFEM with $\alpha = 1.3$ performed as well as the Q4 in the energy norm.

We further investigate the bound properties of the strain energy using the SαFEM with $\alpha_{pref}(h)$. To highlight these properties, the equilibrium element (EQ4) and the compatible element (T3) are also used in the computation. The results are plotted in Fig. 9. It is observed that (1) the solution of SαFEM with any $\alpha \in [1.3, 1.7]$[1] converges to the exact solution; (2) the strain energy of the SαFEM is bounded by the solutions of these two classical models: pure equilibrium (EQ4) and displacement models (T3); (3) the SαFEM solutions using any $\alpha \in [1.3, 1.6]$ are more accurate than those of both the pure equilibrium model and displacement model. Therefore, even if one does not want to find the α_{pref}, one can simply use any $\alpha \in [1.3, 1.6]$ to obtain a more accurate solution than those of two classical models; (4) it is possible to bound the solution by using SαFEM with two αs.

Next, we investigate the volumetric locking issue for the nearly incompressible materials under plane strain condition. Fig. 10 plots the numerical results of the displacements along the neutral axis for a material with the Poisson ratio $\nu = 0.4999$. It is clear that T3 and SαFEM with any α yield poor accuracy. In the contrast, the NS-T3 model gives a good agree-

[1] Theoretically, the SαFEM has been proved to converge for any $\alpha \in [0, \alpha_{cr})$. In application, the range of $\alpha \in [1.3, 1.7]$ gives good performance and provides all the major features of method.

ment with the analytical solution. However, the NS-T3 model is too soft. Therefore, a combined SαFEM/NS-FEM model described in Section 5 can handily avoid volumetric locking for nearly incompressible materials, as shown in Fig. 10. We also found that the domain-based selective ES/NS-FEM model [45] also works very well for incompressible materials, but not as good as the present combined SαFEM/NS-FEM model.

We now analyze in more detail the convergence rates in term of both displacement and energy for some "locking free" models. Figs. 11 and 12 compare, respectively, the convergence of the error norms in displacement and energy of the Sα/NS-FEM (as $\nu = 0.4999$) with the other elements: a selective reduced integration (SRI) technique [1], the quadrilateral equilibrium element (EQ4) and the recently very accurate ES-FEM model [45]. It is found that a superior accuracy and superconvergence is observed for the Sα/NS-FEM at $\alpha_{pref}(h)$.

8.3. Square solid with a circular hole: convergence study

Fig. 13 represents a square 2D solid with a central circular hole of radius $a = 1$ m, subjected to a unidirectional tensile load of $\sigma = 1.0$ N/m at infinity in the x-direction. Due to its symmetry, only the upper right quadrant of the plate is modeled. Plane

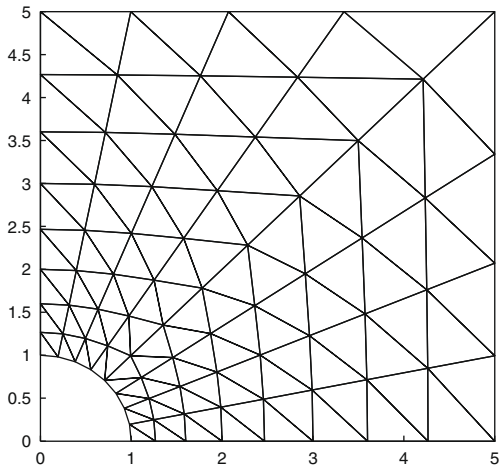

Fig. 14. Domain discretization using 64 quadrilateral (or 128 triangular) elements for the quarter model of the infinite plate with a circular hole.

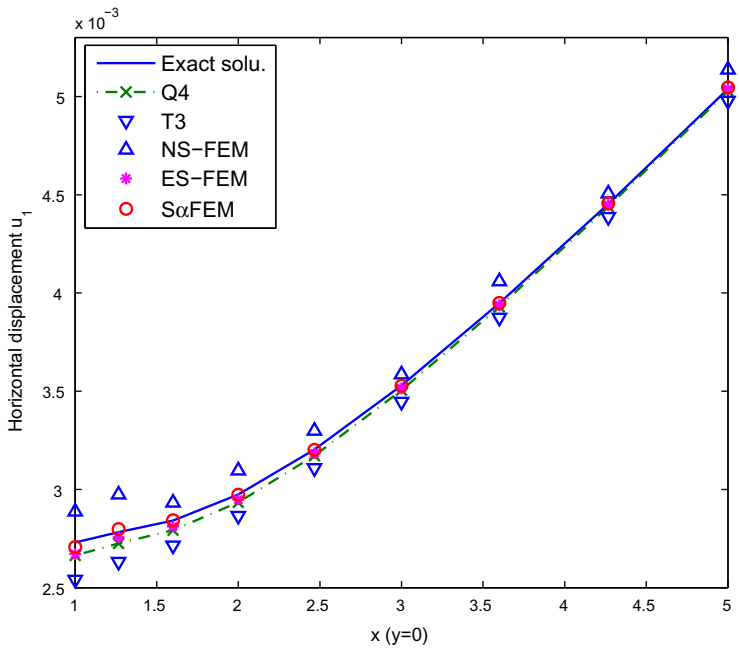

Fig. 15. Horizontal displacement of the infinite plate with a hole along the bottom boundary.

strain condition is assumed and $E = 1.0 \times 10^3$ N/m^2, Poisson ratio $\nu = 0.3$. Symmetric conditions are imposed on the left and bottom edges, and the inner boundary of the hole is traction free. The exact solution of the stress for the corresponding infinite solid is [68]

$$\begin{aligned}
\sigma_{11} &= 1 - \frac{a^2}{r^2}\left[\frac{3}{2}\cos 2\theta + \cos 4\theta\right] + \frac{3a^4}{2r^4}\cos 4\theta \\
\sigma_{22} &= -\frac{a^2}{r^2}\left[\frac{1}{2}\cos 2\theta - \cos 4\theta\right] - \frac{3a^4}{2r^4}\cos 4\theta \\
\tau_{12} &= -\frac{a^2}{r^2}\left[\frac{1}{2}\sin 2\theta + \sin 4\theta\right] + \frac{3a^4}{2r^4}\sin 4\theta
\end{aligned} \tag{57}$$

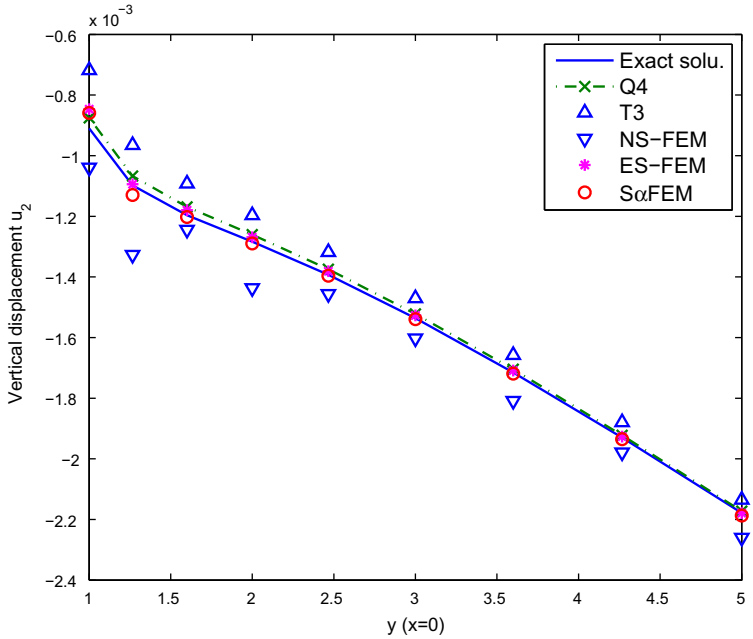

Fig. 16. Vertical displacement of the infinite plate with a hole along the left boundary.

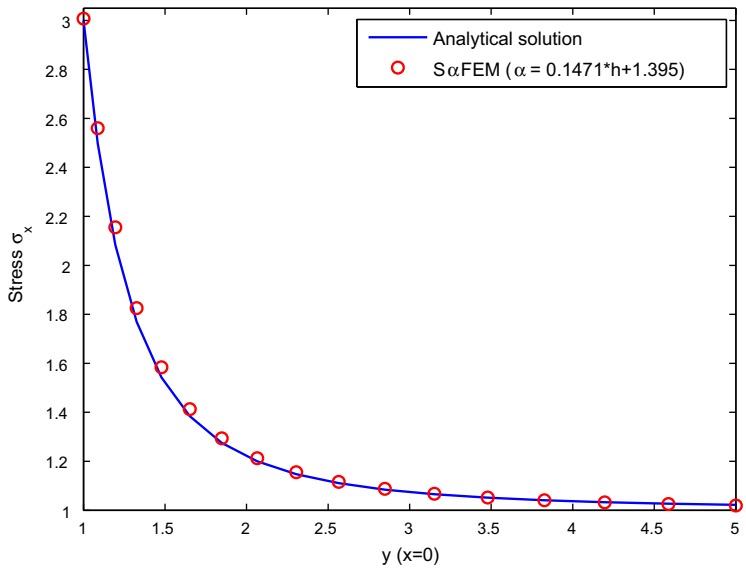

Fig. 17. Distribution of stress along the left boundary ($x = 0$) of the infinite plate with a hole subjected to unidirectional tension.

where (r, θ) are the polar coordinates and θ is measured counterclockwise from the positive x-axis. Traction boundary conditions are imposed on the right ($x = 5.0$) and top ($y = 5.0$) edges based on the exact solution Eq. (57). The displacement components corresponding to the stresses are

$$\begin{aligned} u_1 &= \frac{a}{8\mu}\left[\frac{r}{a}(\kappa+1)\cos\theta + 2\frac{a}{r}((1+\kappa)\cos\theta + \cos 3\theta) - 2\frac{a^3}{r^3}\cos 3\theta\right] \\ u_2 &= \frac{a}{8\mu}\left[\frac{r}{a}(\kappa-1)\sin\theta + 2\frac{a}{r}((1-\kappa)\sin\theta + \sin 3\theta) - 2\frac{a^3}{r^3}\sin 3\theta\right] \end{aligned} \tag{58}$$

where $\mu = E/(2(1+\nu))$,κ is defined in terms of Poisson's ratio by $\kappa = 3 - 4\nu$ for plane strain cases. An illustration of 128 triangular elements is given in Fig. 14.

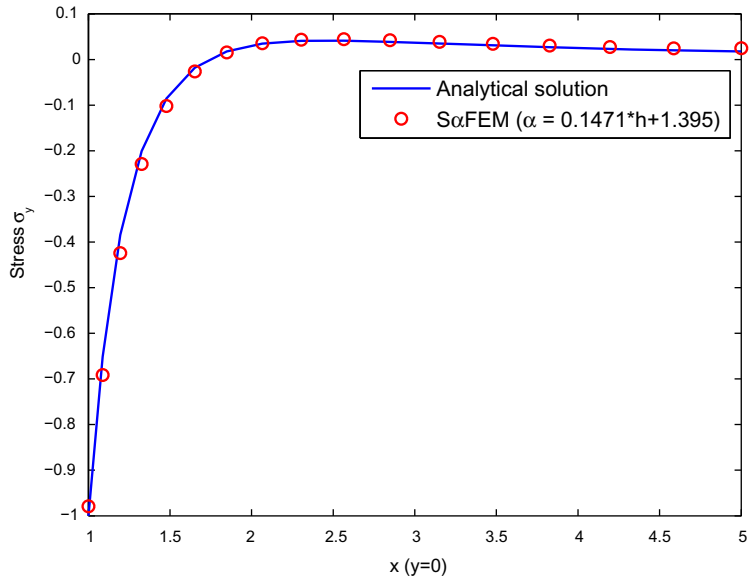

Fig. 18. Distribution of stress along the bottom boundary ($y = 0$) of the infinite plate with a hole subjected to unidirectional tension.

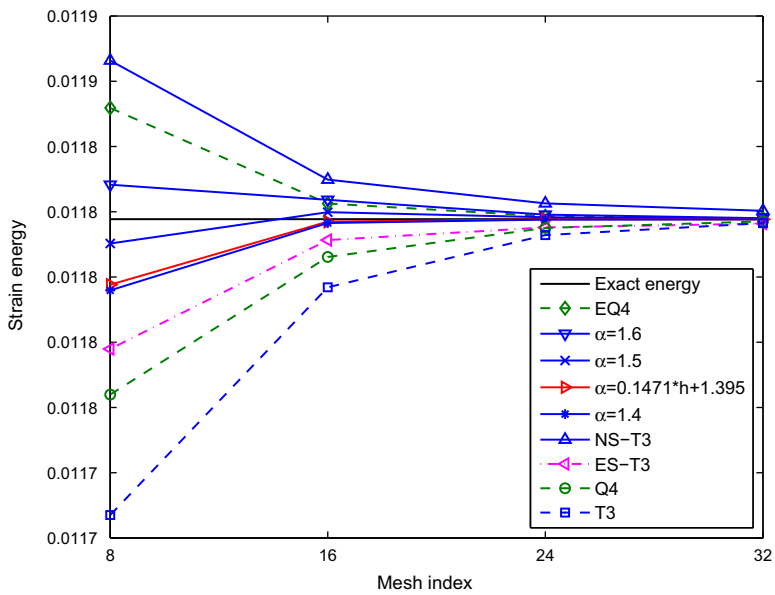

Fig. 19. Solution bounds of energy for infinite plate with a circular hole.

Figs. 15 and 16 illustrate the results for displacements along bottom and left boundaries of the SαFEM (at $\alpha_{pref}(h) = 0.147h + 1.395$), T3, Q4, NS-T3 and ES-T3 using the coarse mesh with 128 triangular elements. It is shown that the SαFEM is a strong competitor of the ES-T3, whereas the T3 and NS-T3 are less accurate. Note that the displacements of the SαFEM at $\alpha = \alpha_{pref}(h)$are even better than those of the Q4. Figs. 17 and 18 exhibit the comparison between the computed stresses using the SαFEM and analytical values. It is observed that the SαFEM solutions are in a good agreement with exact solution and display smooth solutions without using any post-process.

The strain energy curves computed using the SαFEM are plotted in Fig. 19. It is easy to see that the SαFEM has lower bound ($\alpha = 1.4$) and upper bound ($\alpha = 1.6$) compared to the exact solution. As expected, the FEM models behave over-stiffly and hence give lower bounds, while the equilibrium element (EQ4) and NS-T3 behave over-softly and give upper bounds. Using the SαFEM, we can obtain a quite close-to-exact stiffness, and hence the very accurate results are achieved when $\alpha = \alpha_{pref}(h)$. Figs. 20 and 21 plot the convergence rates for the error in displacement and energy using

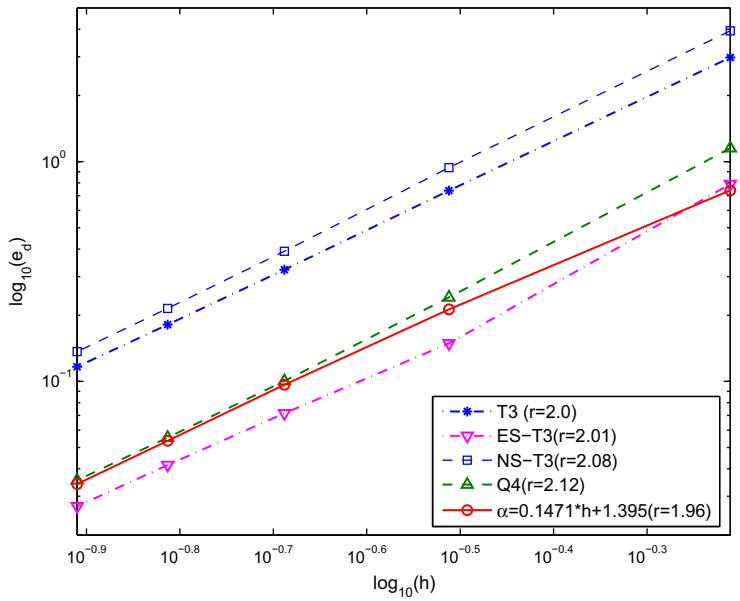

Fig. 20. Convergence and the estimated rate in the displacement norm of the infinite plate with a circular hole.

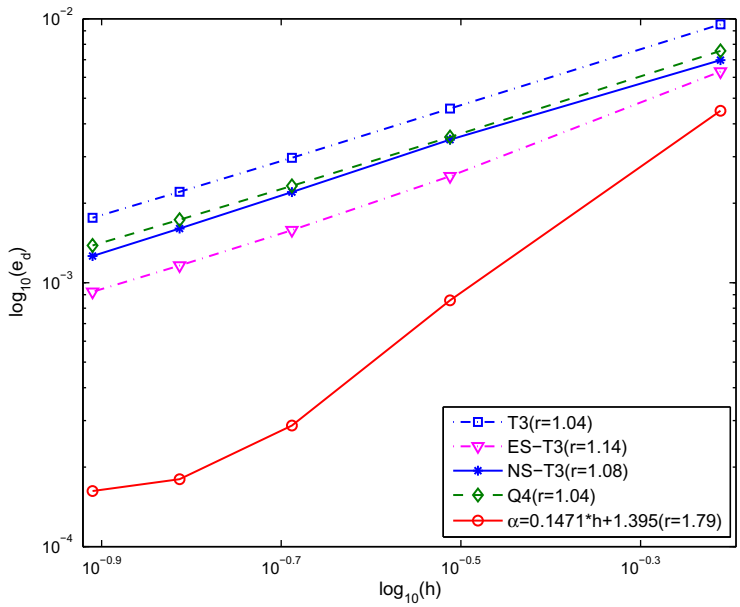

Fig. 21. Convergence and the estimated rate in the energy norm of the infinite plate with a circular hole.

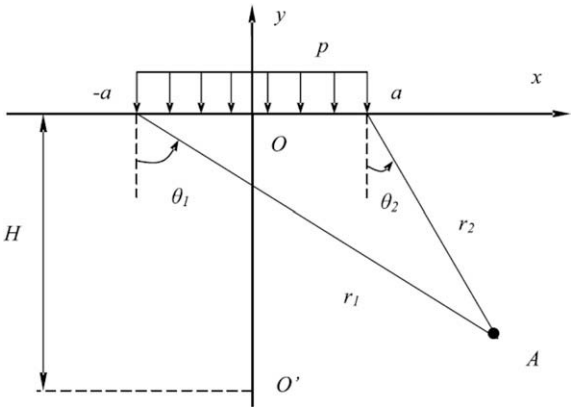

Fig. 22. Semi-infinite plane subjected to a uniform pressure.

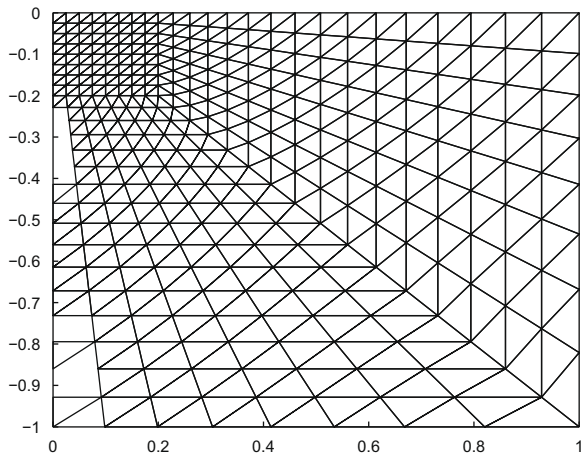

Fig. 23. Domain discretization of the semi-infinite plane problem using triangular elements.

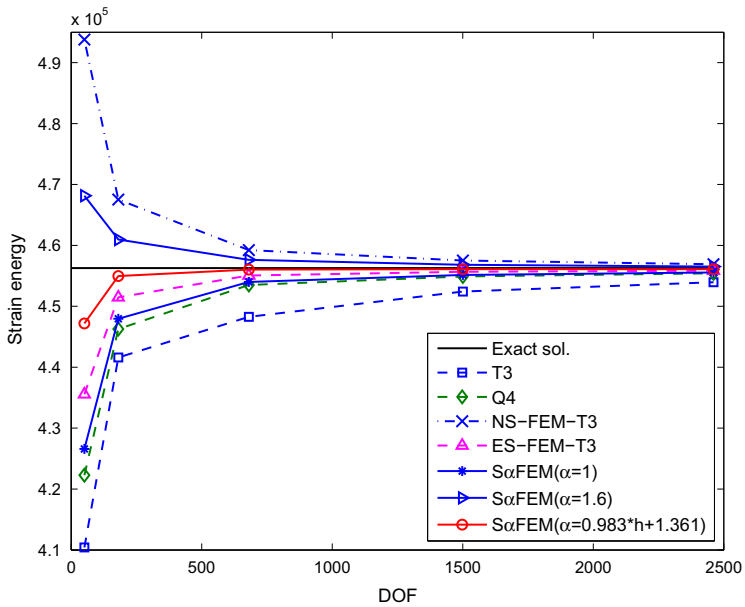

Fig. 24. Strain energy for the semi-infinite plane problem.

$\alpha_{pref}(h) = 0.147h + 1.395$. It is observed that (1) the present SαFEM is, respectively, about 3.5 (for displacement norm) and 8.2 (for energy norm) times more accurate than T3 and even more accurate than Q4; (2) a superconvergent solution is obtained for the SαFEM in energy norm; (3) the SαFEM stands out clearly in energy norm measure.

8.4. Semi-infinite plane: convergence study

The semi-infinite plane shown in Fig. 22 is studied subjected to a uniform pressure within a finite range ($-a \leqslant x \leqslant a$). The plane strain condition is considered. The analytical stresses are given by [68]

$$\begin{aligned}
\sigma_{11} &= \frac{p}{2\pi}[2(\theta_1 - \theta_2) - \sin 2\theta_1 + \sin 2\theta_2] \\
\sigma_{22} &= \frac{p}{2\pi}[2(\theta_1 - \theta_2) + \sin 2\theta_1 - \sin 2\theta_2] \\
\tau_{12} &= \frac{p}{2\pi}[\cos 2\theta_1 - \cos 2\theta_2]
\end{aligned} \tag{59}$$

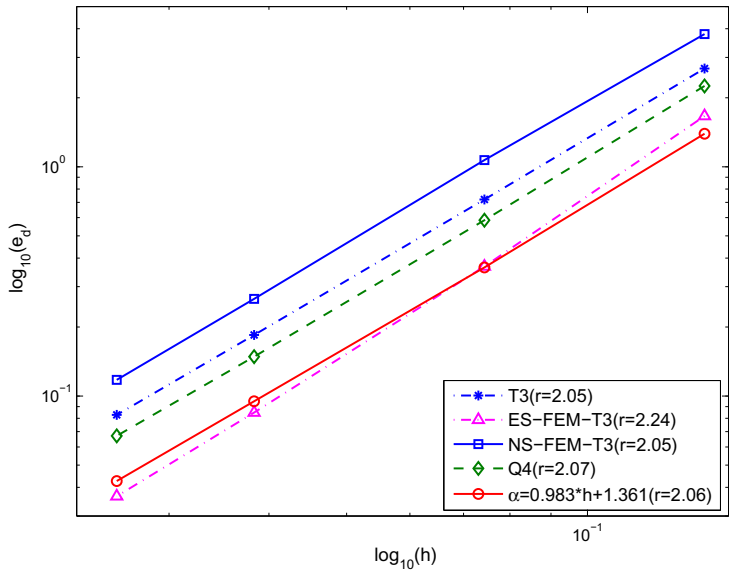

Fig. 25. Convergence and the estimated rate in displacement norm for the semi-infinite plane problem.

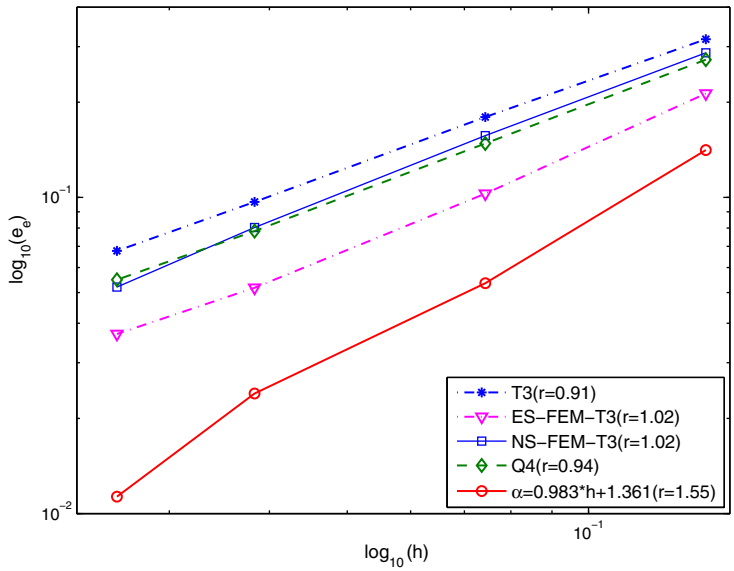

Fig. 26. Convergence and the estimated rate in energy norm for the semi-infinite plane problem.

The directions of and are indicated in Fig. 22. The corresponding displacements can be expressed as

$$\begin{aligned} u_1 &= \frac{p(1-\nu^2)}{\pi E}\left[\frac{1-2\nu}{1-\nu}[(x+a)\theta_1-(x-a)\theta_2]+2y\ln\frac{r_1}{r_2}\right] \\ u_2 &= \frac{p(1-\nu^2)}{\pi E}\left[\frac{1-2\nu}{1-\nu}\left[y(\theta_1-\theta_2)+2H\arctan\frac{1}{c}\right]+2(x-a)\ln r_2--2(x+a)\ln r_1+4a\ln a+2a\ln(1+c^2)\right] \end{aligned} \tag{60}$$

where $H = ca$ is the distance from the origin to point O', the vertical displacement is assumed to be zero and c is a coefficient.

Due to the symmetry about the y-axis, the problem is modeled with a square width. The left and bottom sides are constrained using the exact displacements given by Eq. (60) while the right side is subjected to tractions computed from Eq. (59). Fig. 23 gives the discretization of the domain using triangular elements.

Again, it is found from Fig. 24 that (1) the upper and lower bound properties on the strain energy of the SαFEM have been obtained; (2) the SαFEM with $\alpha_{pref}(h)$ is superior to all the other models including the ES-T3. We also note the solution of the SαFEM ($\alpha = 1$) is even more accurate than that of Q4 for this problem. The convergence rate of the errors in displacement and energy is evaluated and represented in Figs. 25 and 26. It is shown that the SαFEM with$\alpha_{pref}(h)$ is about 3.4 (for displacement node) and 5.3 (for energy norm) times more accurate than T3 and about 4 times more accurate than the Q4. Superconvergence is also observed for the SαFEM: the convergence rate of $r = 1.55$ is larger than the theoretical value of 1.0 in energy norm.

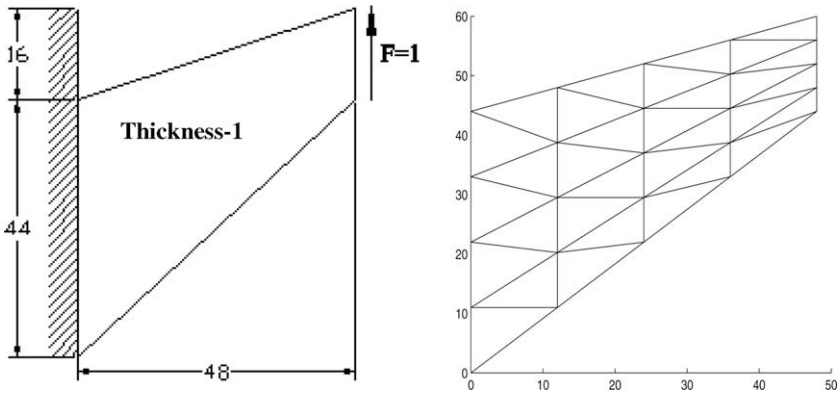

Fig. 27. Cook's membrane problem and its discretization using the coarse mesh.

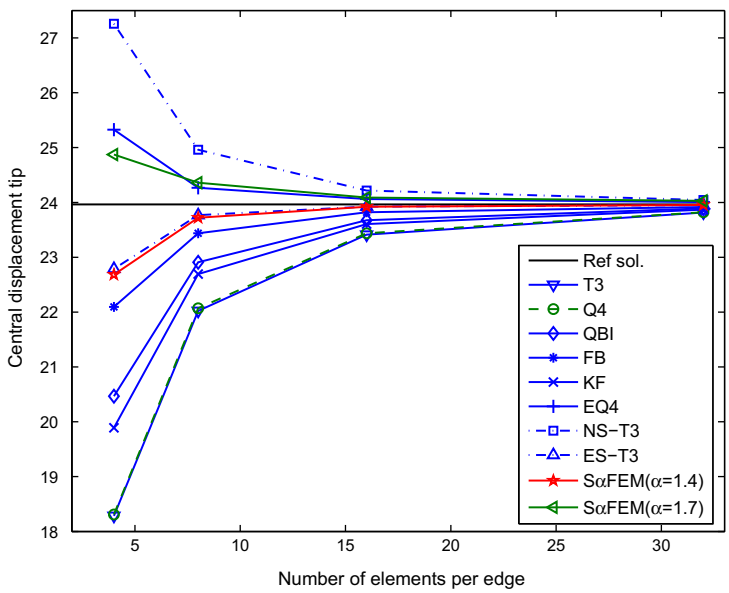

Fig. 28. Comparison of displacement tip for Cook's membrane ($\nu = 1/3$).

8.5. Cook's membrane: test for bending behavior and volumetric locking

This benchmark problem, shown in Fig. 27, is a well known Cook's membrane problem designed for testing a numerical method in simulating bending behavior as well as volumetric locking [69]. The problem refers to a clamped tapered panel subjected to an in-plane shearing load, resulting in deformation dominated by a bending deformation. The computation is performed under the plane stress condition, Young's modulus $E = 1$ and Poisson's ratio $\nu = 1/3$. The exact solution of the problem is unknown. The reference value of the vertical displacement at center tip section is found to be 23.9642 [65] and the reference value of the strain energy is 12.015 [70].

Fig. 28 compares the result of displacement tip of the SαFEM with eight published 4-node quadrilateral elements: Q4-standard isoparametric 2×2 quadrature Gauss points, FB-one Gauss point with hourglass stabilization [71], QBI-Quintessential bending/incompressible element [53], KF-one Gauss point with hourglass control [72], the quadrilateral equilibrium

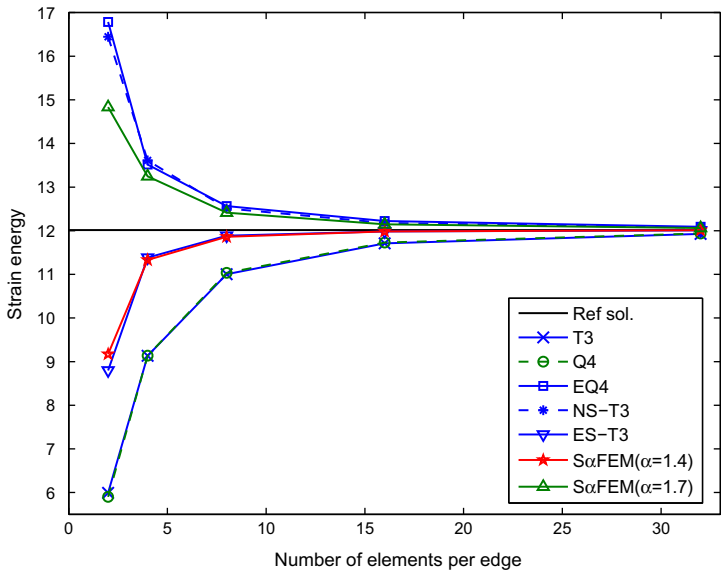

Fig. 29. Solution bounds of strain energy for Cook's membrane.

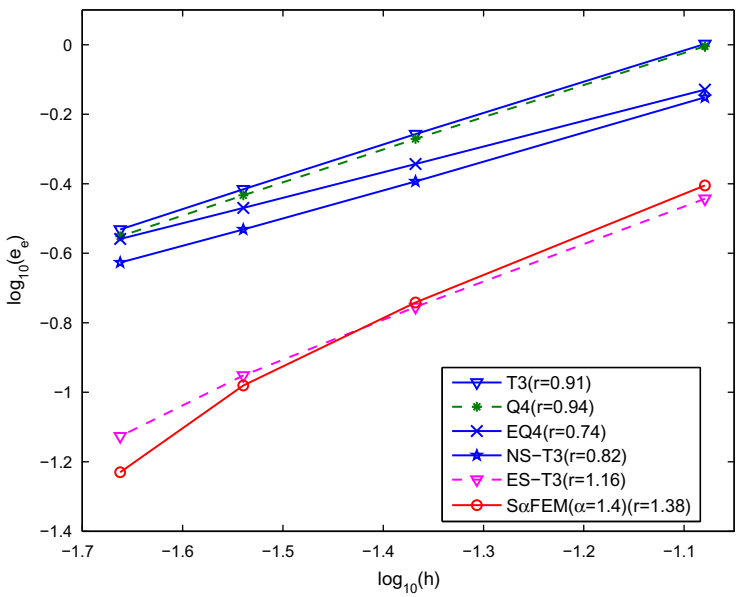

Fig. 30. Convergence and the estimated rate in energy error for Cook's membrane.

element (EQ4), a nodal-based smoothed FEM using triangular mesh (NS-T3) and an edge-based smoothed FEM using triangular mesh (ES-T3). It can be seen that (1) the result of the SαFEM at $\alpha = 1.4$ is much more accurate than all those of other elements with coarse meshes; (2) a very tight solution bounds can be given using $\alpha = 1.4$ and $\alpha = 1.7$.

The convergence of the strain energy is exhibited in Fig. 29, and the convergence rate of the error norm in energy is shown in Fig. 30. The results shows again the superiority of the present SαFEM to other models, and it is about eight times more accurate that both the T3 and Q4 in energy norm.

We now consider further the case of nearly incompressible material with $\nu = 0.4999999$ in the plane strain condition. As shown in Fig. 31, the SαFEM at $\alpha = 1.4$ gives again much more accurate solution compared to all the others elements such as QBI element [53], ASMD, ASQBI, ASOI elements [54] of FEM models.

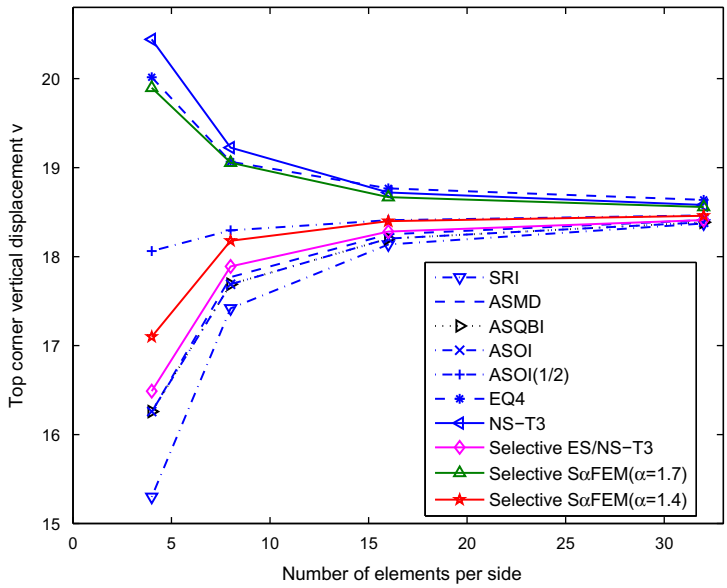

Fig. 31. Comparison of displacement tip for Cook's membrane ($\nu = 0.4999999$).

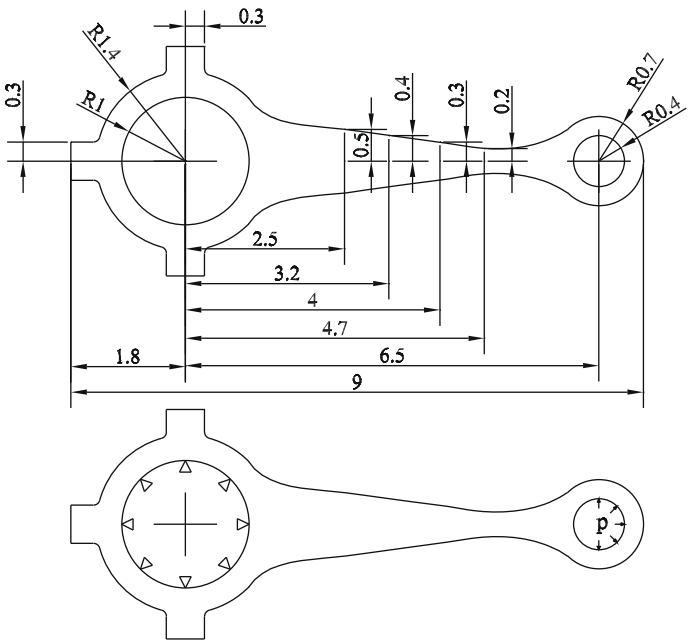

Fig. 32. Geometric model and boundary conditions of an automobile connecting bar.

8.6. A connecting rod: automobile part

This example performs a static stress analysis of an automobile part as a part of an actual industry project. The connecting bar has a relatively complicated geometry, and it is difficult in generating meshes using quadrilateral elements, and hence we use only triangular elements that can be generated with ease for all the models. The boundary conditions as well as the applied load are demonstrated as shown in Fig. 32 with $p = 1$ MPa. Plane stress problem is considered with elastic modulus $E = 10$ GPa and Poisson's ratio $\nu = 0.3$.

Fig. 33 shows the discretization of the domain using 3 meshes (116, 373 and 1321 nodes) with triangular elements. As analytical solutions are unavailable, a reference solution of strain energy of 331.17656 is computed using the T3 with as many as 22788 nodes. Fig. 34 illustrates the strain energy of the SαFEM for several α-values. It is shown again that the SαFEM can produce upper bound (with $\alpha = 1.7$) or lower bound (with $\alpha = 1.5$) solutions in energy norm by an adjustable parameter α. The convergence rate of the SαFEM for two α-values plotted in Fig. 35 is clearly superior to others elements of FEM models.

Singularity cases

We next apply the present SαFEM to analyze two problems with different orders of singularity: L-shaped panel subjected to tractions and a rectangular panel with an edged crack subjected to tension.

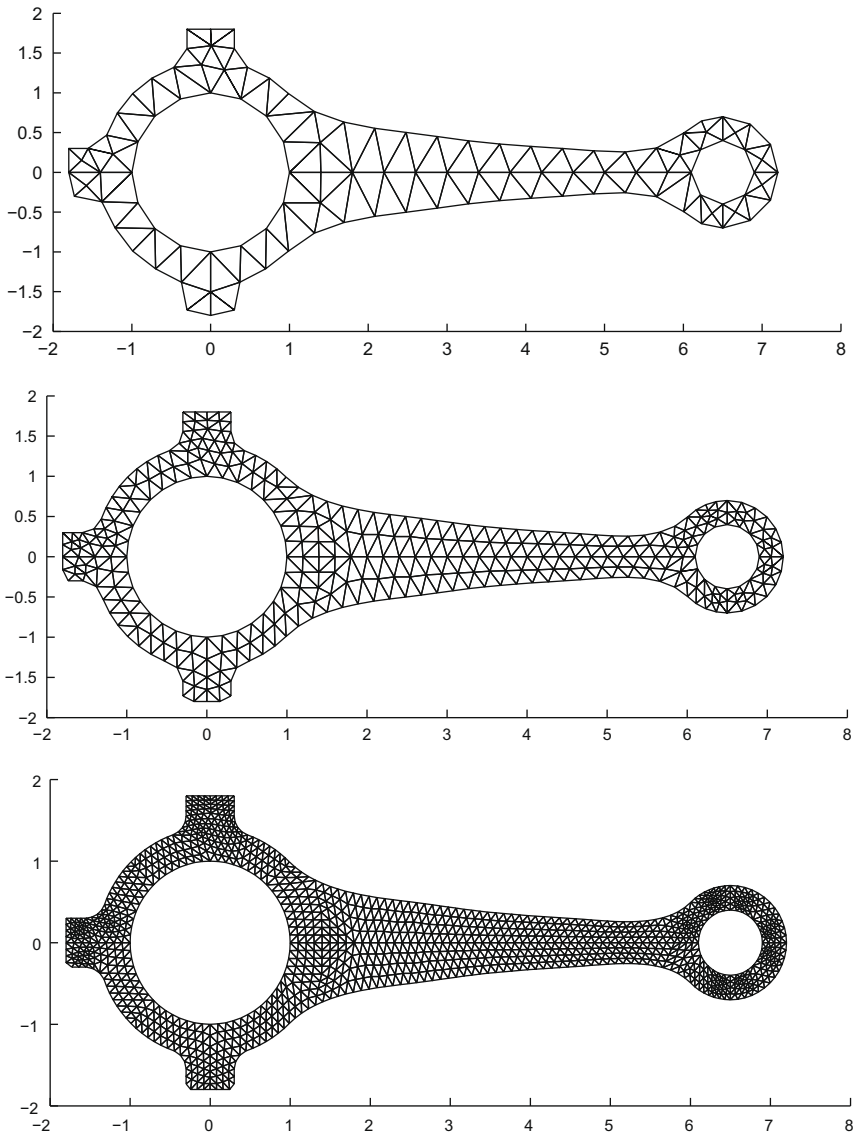

Fig. 33. Domain discretization of the connecting bar using three meshes (a) Mesh 1 (116 nodes); (b) Mesh 2 (373 nodes); (c) Mesh 3 (1321 nodes).

8.7. L-shaped panel subjected tractions: Re-entrant corner singularity

Consider an L-shaped panel under plane stress condition with applied tractions and boundary conditions as shown in Fig. 36. The parameters of the structure are $E = 1.0$, $\nu = 0.3$, $t = 1$. In this problem, the re-entrant corner possesses a stress singularity.

The exact strain energy of this problem is not available. However, it can be estimated through the procedure of Richardson's extrapolation for the displacement models and equilibrium models [41,42]. The estimated precision is determined by the mean value of these two extrapolated strain energies. The reference strain energy given in [73] is approximately 15566.460 and is used to estimate the convergence rate of all elements.

The convergence of the strain energy is exhibited in Fig. 37, and the convergence rates are plotted in Fig. 38. It is clear that the SαFEM can provide the upper and lower bound properties on the strain energy by choosing a parameter $\alpha \in [1.3, 1.5]$, see Fig. 37. Using the procedure given in Section 7 to compute α_{pref}, the best possible solution is obtained at

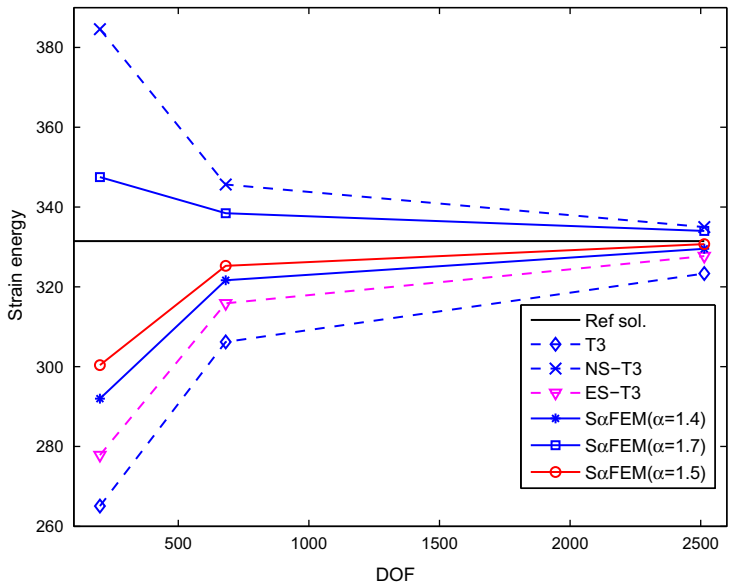

Fig. 34. Strain energy for different values α of the connecting rod.

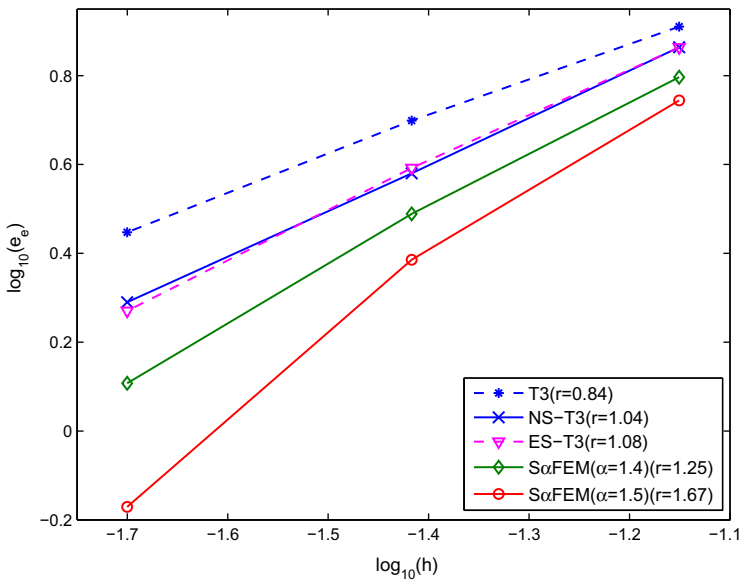

Fig. 35. Convergence and the estimated rate in energy norm for the connecting rod.

$\alpha_{pref} = 0.6582h + 1.4119$. As shown in Figs. 37 and 38, the accuracy of the SαFEM with $\alpha_{pref}(h)$ is very high and is superior to all the other models including the ES-FEM. We also note that the strain energy of the SαFEM ($\alpha = 1.3$) is even more accurate than that of ES-FEM for this problem. The convergence rate of the SαFEM is nearly superconvergent ($r = 1.1$) at α_{pref} because of the stress singularity. In addition, an adaptive approach in the vicinity of the corner may be useful to reduce the error and significantly enhance the computational effect.

8.8. Rectangular panel with an edged crack subjected to tension: strong singularity case

Consider now a fracture problem of a rectangular panel with an edged crack subject to tension as shown in Fig. 39. The input data for this problem are $E = 1.0\ \mathrm{N/m^2}$, $\nu = 0.3$, $t = 1$ m. Only half of domain is modeled in the present SαFEM with uniform meshes of the same aspect ratio. By incorporating the dual analysis [41,42] and the procedure of Richardson's extrapolation with very fine meshes, Beckers et al. [73] proposed the best possible approximation of the exact strain energy to be

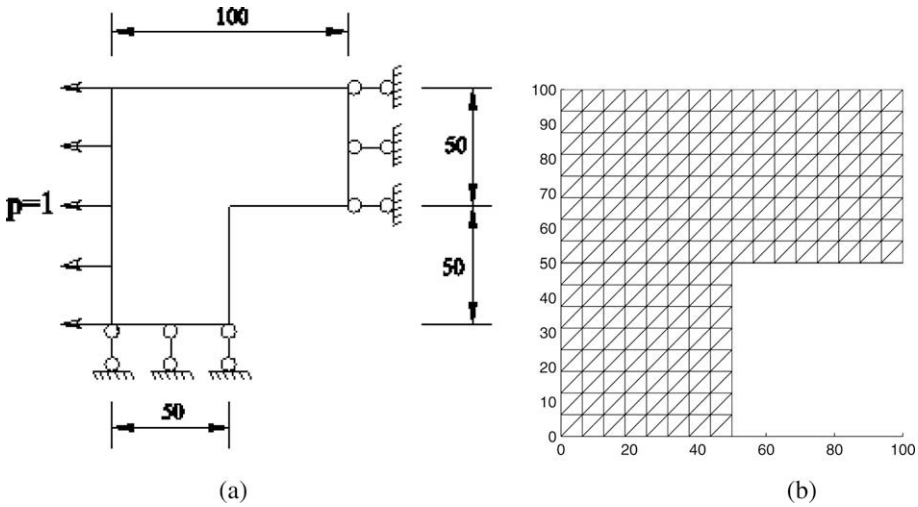

Fig. 36. L-shaped panel and its discretization using the uniform coarse mesh of 384 triangular elements.

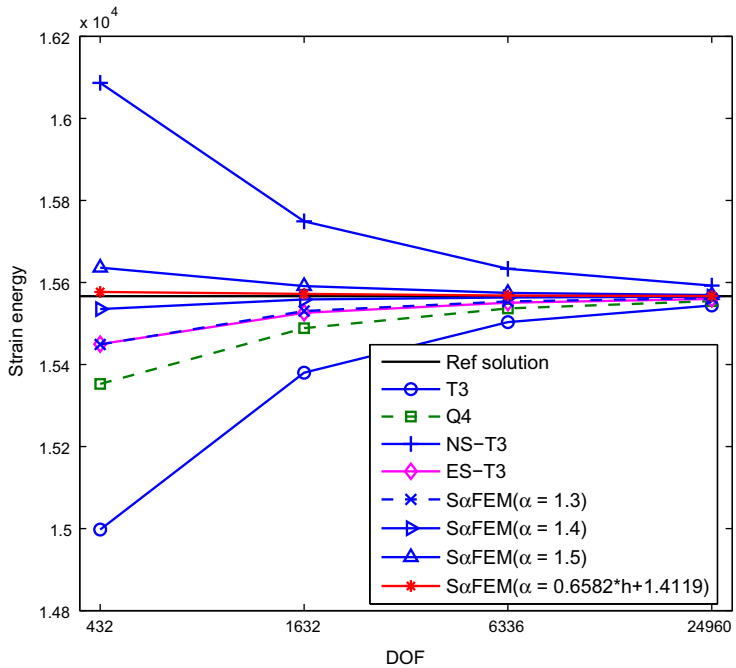

Fig. 37. Upper and lower bounds of strain energy for the L-shaped panel problem.

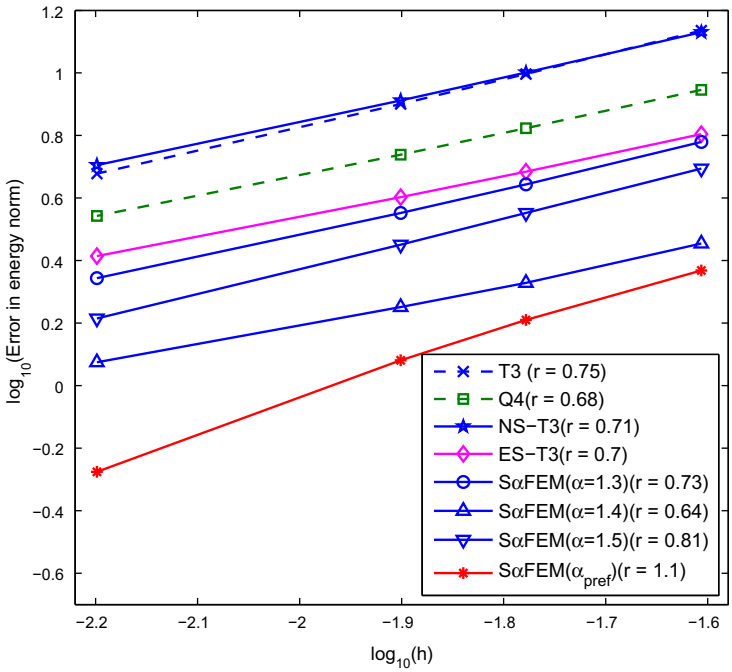

Fig. 38. Convergence and the estimated rate in energy norm for the L-shaped panel problem.

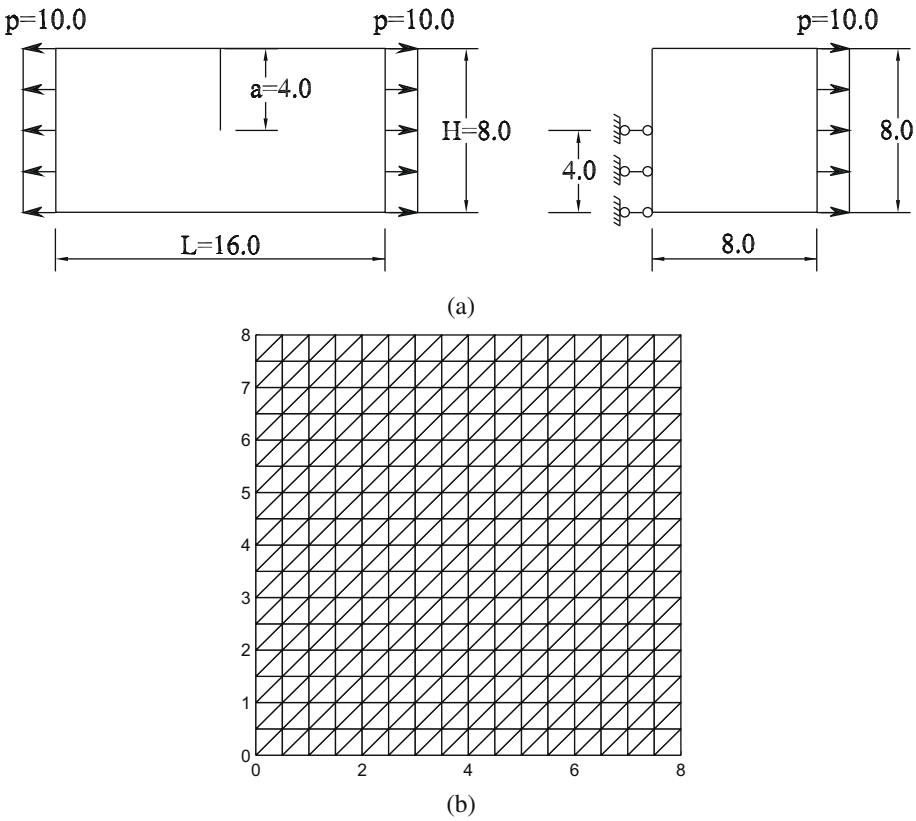

Fig. 39. (a) Fracture problem and the half model; (b) The uniform coarse mesh of 128 triangular elements.

8085.7610. Fig. 40 plots the convergence of the strain energy, and the convergence rates are shown in Fig. 41. It is shown that the upper and lower bound properties on the strain energy are completely achieved by manipulating a parameter $\alpha \in [1.3, 1.6]$. Using the procedure given in Section 7, α_{pref} is proposed for the best possible solution to be $\alpha_{pref} = 0.0115h + 1.5652$. The results given in Figs. 40 and 41 show that the solution of the SαFEM is very accurate compared to all the other models and the convergence rate ($r = 0.94$) of the SαFEM at $\alpha_{pref}(h)$ is nearly twice the convergence rate derived from the conforming FEM approaches and others models. Again, the strain energy of the SαFEM ($\alpha = 1.3$) is also more accurate than that of ES-FEM. In

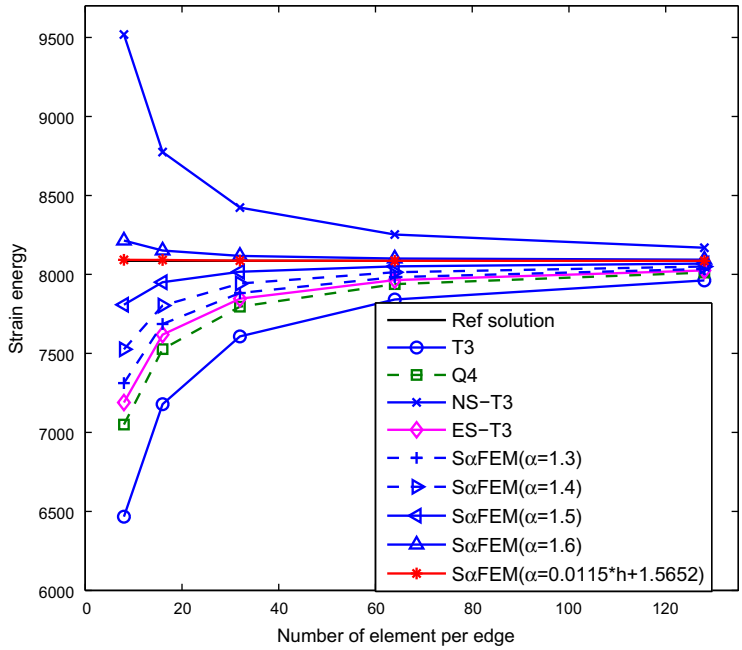

Fig. 40. Solution in strain energy for fracture problem.

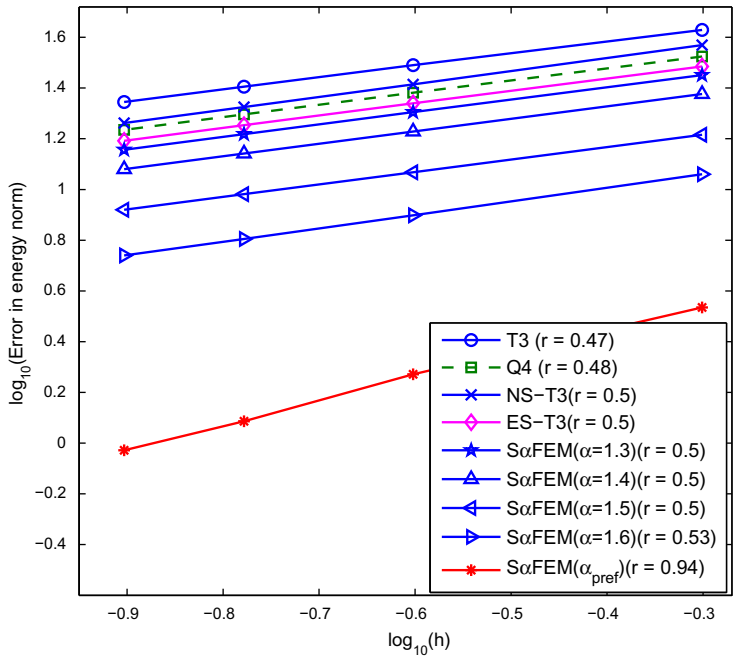

Fig. 41. Convergence and the estimated rate in energy norm for the crack edge rectangular plate.

addition, due to the strong singularity at a crack tip, the incorporation of the SαFEM with XFEM [33–35,38] may be very useful to analyze fracture mechanics problems.

9. Computational efficiency and condition number of stiffness matrix

Now we mention the computational efficiency of present method compared with other methods. Owing to the establishment of the assumed strain field in Eq. (9), no additional degrees of freedom are necessary. Without lose of generality, let us consider the computational efficiency for the cantilever beam. Figs. 42 and 43 illustrate the errors in displacement and energy norms against the CPU time (seconds). It is observed that the computation time of the SαFEM is longer than those of the Q4 and the T3, the ES-T3 and as same as that of the NS-T3. The reason is due to the additional time required for the additional

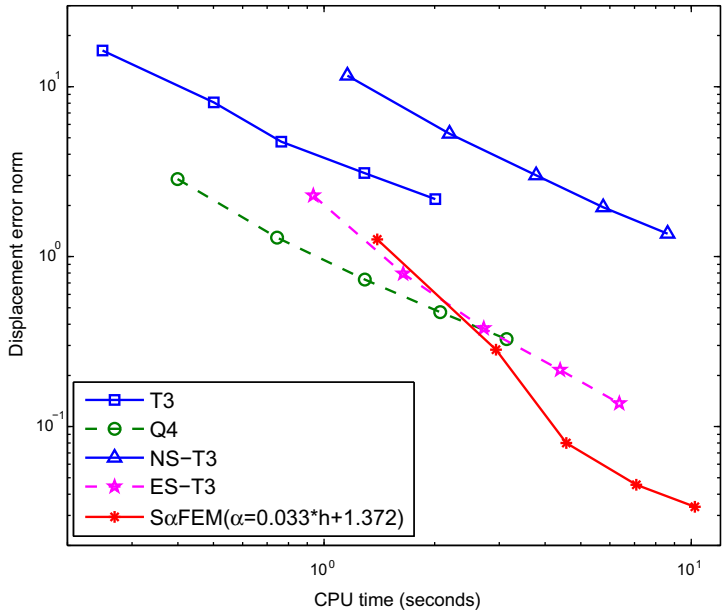

Fig. 42. Comparison of the computational efficiency in displacement error norm for a cantilever beam.

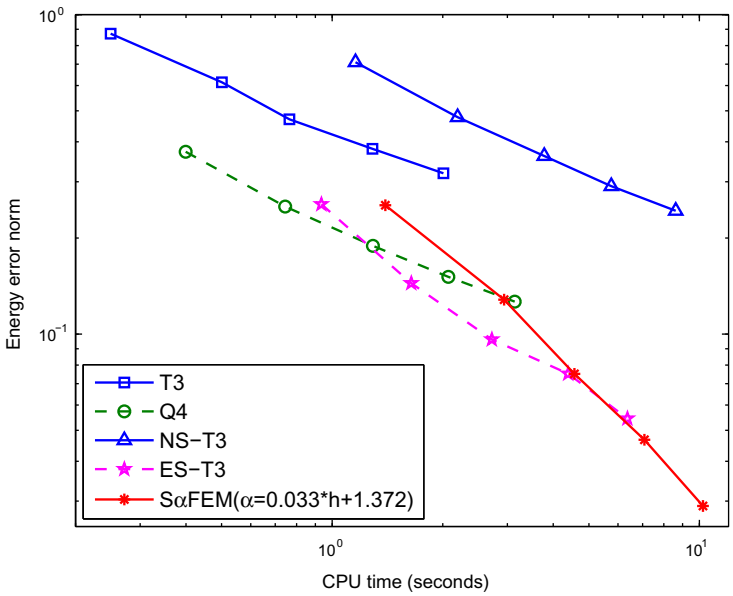

Fig. 43. Comparison of the computational efficiency in energy error norm for a cantilever beam.

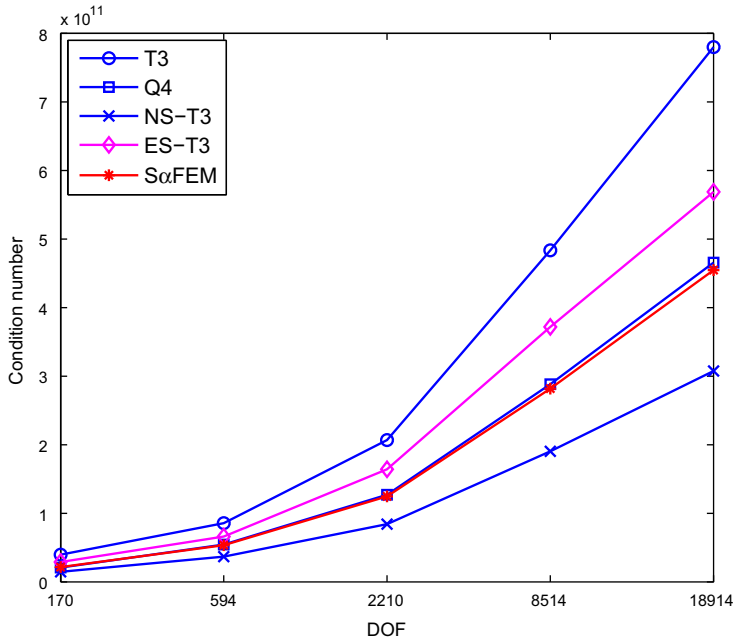

Fig. 44. An illustration of the condition number of the stiffness matrix for a cantilever beam.

assessment and assemblage of nodal stiffness matrix in (29). However, considering the computational efficiency (computation time for the same accuracy) in terms of displacement and energy error norms, the SαFEM is more effective.

We have also checked the condition number of stiffness matrix. As shown from Fig. 44, the condition number of the SαFEM stiffness matrix is roughly the same as those of the standard FEM-Q4 element. This implies that the SαFEM should be as stable and the FEM-Q4 model.

10. Conclusion

This paper presents carefully a designed procedure to modify the piecewise constant strain field of linear triangular FEM models, and to reconstruct a strain field with an adjustable parameter α. The new Galerkin-like weakform proposed is simple and possesses the same good properties of the standard Galerkin weak form. A superconvergent alpha finite element method (SαFEM) for solid mechanics problems is then formulated by using the modified strain field and the weak form. Important properties of the present method are properly proven theoretically, and confirmed numerically. The method has the following attractive features: (1) it is variationally consistent because the weak form are derived from the Hellinger–Reissner variational principle; (2) the SαFEM can always provide both lower and upper bounds to the exact solution in energy norm for all elasticity problems by properly choosing $\alpha \in [0, \alpha_{cr})$; for all the example problems tested in this paper, $\alpha = 1.3$ always gives a lower bound, and $\alpha = 1.7$ gives an upper bound; (3) it always produces a superconvergent solution for an $\alpha \in [1.3, 1.7]$, and very accurate and superconvergent solution can be found using $\alpha_{pref}(h)$ that can be found via simple steps for a given problem; (4) Volumetric locking is overcome by using a novel technique of model-based selective Sα/NS-FEM; (5) Finally, the SαFEM is easy to implement into a finite element program using triangular meshes that can be generated with ease for complicated problem domains.

In addition, it is promising to extend the present method for the 3D problems and the plate and shell problems by combining the SαFEM with DSG method [74] to get rid of shear locking and to improve the accuracy of solutions. It is also promising to maintain accuracy in a local region and to improve the rough solution of strong discontinuities in fracture structures by coupling the SαFEM with the extended finite element method (XFEM) [33–35,38].

References

[1] T.J.R. Hughes, The Finite Element Method: Linear Static and Dynamic Finite Element Analysis, Prentice-Hall, 1987.
[2] O.C. Zienkiewicz, R.L. Taylor, The Finite Element Method, fifth ed., Butterworth Heinemann, Oxford, 2000.
[3] G.R. Liu, S.S. Quek, The Finite Element Method: A Practical Course, Butterworth Heinemann, Oxford, 2003.
[4] G.R. Liu, A weakened weak (W2) form for a unified formulation of compatible and incompatible methods, part I-Theory and part II-Application to solid mechanics problems, Int. J. Numer. Methods Eng., in press, 2009.
[5] G.R. Liu, A generalized gradient smoothing technique and the smoothed bilinear form for Galerkin formulation of a wide class of computational methods, Int. J. Comput. Methods 5 (2) (2008) 199–236.
[6] D.J. Allman, A compatible triangular element including vertex rotations for plane elasticity analysis, Comput. Struct. 19 (1984) 1–8.

[7] P.G. Bergan, C.A. Felippa, A triangular membrane element with rotational degrees of freedom, Comput. Methods Appl. Mech. Eng. 50 (1985) 25–69.
[8] D.J. Allman, Evaluation of the constant strain triangle with drilling rotations, Int. J. Numer. Methods Eng. 26 (1988) 2645–2655.
[9] C.A. Felippa, A study of optimal membrane triangular with drilling freedoms, Comput. Methods Appl. Mech. Eng. 192 (2003) 2125–2168.
[10] R. Piltner, R.L. Taylor, Triangular finite elements with rotational degrees of freedom and enhanced strain modes, Comput. Struct. 75 (2000) 361–368.
[11] T. Rong, Y. Genki, Allman's triangle, rotational DOF and partition of unity, Int. J. Numer. Methods Eng. 69 (2007) 837–858.
[12] J.C. Simo, M.S. Rifai, A class of mixed assumed strain methods and the method of incompatible modes, Int. J. Numer. Methods Eng. 29 (1990) 1595–1638.
[13] U. Andelfinger, E. Ramm, EAS-elements for two-dimensional threedimensional plate and shells and their equivalence to HR-elements, Int. J. Numer. Methods Eng. 36 (1993) 1413–1449.
[14] S.T. Yeo, B.C. Lee, Equivalence between enhanced assumed strain method and assumed stress hybrid method based on the Hellinger–Reissner principle, Int. J. Numer. Methods Eng. 39 (1996) 3083–3099.
[15] M. Bischoff, E. Ramm, D. Braess, A class equivalent enhanced assumed strain and hybrid stress finite elements, Comput. Mech. 22 (1999) 444–449.
[16] J.M.A. César de Sá, R.M. Natal Jorge, New enhanced strain elements for incompatible problems, Int. J. Numer. Methods Eng. 44 (1999) 229–248.
[17] J.M.A. César de Sá, RM. Natal Jorge, R.A. Fontes Valente, P.M. A Areias, Development of shear locking-free shell elements using an enhanced assumed strain formulation, Int. J. Numer. Methods Eng. 53 (2002) 1721–1750.
[18] R.P.R. Cardoso, J.W. Yoon, Mahardika, S. Choudhry, R.J. Alves de Sousa, R.A. Fontes Valente, Enhanced assumed strain (EAS) and assumed natural strain (ANS) methods for one-point quadrature solid-shell elements, Int. J. Numer. Methods Eng. 75 (2008) 156–187.
[19] T.H.H. Pian, C.C. Wu, Hybrid and Incompatible Finite Element Methods, CRC Press, Boca Raton, FL, 2006.
[20] G.R. Liu, G.Y. Zhang, K.Y. Dai, Y.Y. Wang, Z.H. Zhong, G.Y. Li, X. Han, A linearly a u conforming point interpolation method (LC-PIM) for 2D solid mechanics problems, Int. J. Comput. Methods 2 (2005) 645–665.
[21] G.R. Liu, Y.T. Gu, A point interpolation method for two-dimensional solids, Int. J. Numer. Methods Eng. 50 (2001) 937–951.
[22] J.G. Wang, G.R. Liu, A point interpolation meshless method based on radial basis functions, Int. J. Numer. Methods Eng. 54 (2002) 1623–1648.
[23] J.S. Chen, C.T. Wu, S. Yoon, Y. You, A stabilized conforming nodal integration for Galerkin mesh-free methods, Int. J. Numer. Methods Eng. 50 (2001) 435–466.
[24] G.R. Liu, K.Y. Dai, T.T. Nguyen, A smoothed element method for mechanics problems, Comput. Mech. 39 (2007) 859–877.
[25] G.R. Liu, T.T. Nguyen, K.Y. Dai, K.Y. Lam, Theoretical aspects of the smoothed finite element method (SFEM), Int. J. Numer. Methods Eng. 71 (2007) 902–930.
[26] Hung Nguyen-Xuan, Stéphane Bordas, Hung Nguyen-Dang, Smooth finite element methods: convergence, accuracy and properties, Int. J. Numer. Methods Eng. 74 (2008) 175–208.
[27] Dai KY, Liu GR, Nguyen TT, An n-sided polygonal smoothed finite element method (nSFEM) for solid mechanics, Finite Elem. Anal. Des. 43 (2007) 847–860.
[28] K.Y. Dai, G.R. Liu, Free and forced vibration analysis using the smoothed finite element method (SFEM), J. Sound Vib. 301 (2007) 803–820.
[29] H. Nguyen-Xuan, T. Rabczuk, S. Bordas, J.F. Debongnie, A smoothed finite element method for plate analysis, Comput. Methods Appl. Mech. Eng. 197 (2008) 1184–1203.
[30] H. Nguyen-Xuan, T. Nguyen-Thoi, A stabilized smoothed finite element method for free vibration analysis of Mindlin–Reissner plates, Commun. Numer. Methods Eng., in press, doi:10.1002/cnm.1137.
[31] N. Nguyen-Thanh, T. Rabczuk, H. Nguyen-Xuan, S. Bordas, A smoothed finite element method for shell analysis, Comput. Methods Appl. Mech. Eng. 198 (2008) 165–177.
[32] X.Y. Cui, G.R. Liu, G.Y. Li, X. Zhao, T. Nguyen-Thoi, G.Y. Sun, A smoothed finite element method (SFEM) for linear and geometrically nonlinear analysis of plates and shells, CMES-Comput. Model. Eng. Sci. 28 (2) (2008) 109–125.
[33] N. Moes, J. Dolbow, T. Belytschko, A finite element method for crack growth without remeshing, Int. J. Numer. Methods Eng. 46 (1) (1999) 131–150.
[34] T. Belytschko, N. Moes, S. Usui, C. Parimi, Arbitrary discontinuities in finite elements, Int. J. Numer. Methods Eng. 50 (2001) 993–1013.
[35] S. Bordas, P.V. Nguyen, C. Dunant, A. Guidoum, H. Nguyen-Dang, An extended finite element library, Int. J. Numer. Methods Eng. 71 (6) (2007) 703–732.
[36] J.M. Melenk, I. Babuška, The partition of unity finite element method: basic theory and applications, Comput. Methods Appl. Mech. Eng. 139 (1–4) (1996) 289–314.
[37] I. Babuška, J.M. Melenk, The partition of unity method, Int. J. Numer. Methods Eng. 40 (4) (1997) 727–758.
[38] S. Bordas, T. Rabczuk, H. Nguyen-Xuan, P. Nguyen Vinh, S. Natarajan, T. Bog, Q. Do Minh, H. Nguyen Vinh, Strain smoothing in FEM and XFEM, Comput. Struct., in press, doi:10.1016/j.compstruc.2008.07.006.
[39] G.R. Liu, T. Nguyen-Thoi, H. Nguyen-Xuan, K.Y. Lam KY, A node-based smoothed finite element method (NS-FEM) for upper bound solutions to solid mechanics problems, Comput. Struct. 87 (2009) 14–26.
[40] G.R. Liu, G.Y. Zhang, Upper bound solution to elasticity problems: a unique property of the linearly conforming point interpolation method (LC-PIM), Int. J. Numer. Methods Eng. 74 (2008) 1128–1161.
[41] B.M. Fraeijs de Veubeke, Displacement and equilibrium models in the finite element method, in: O.C. Zienkiewicz, G. Holister (Eds.), Stress Analysis, John Wiley and Sons, Berlin, 1965, pp. 15–197. Chapter 9, Reprinted in Int. J. Numer. Methods Eng. 52 (2001) 287–342.
[42] J.F. Debongnie, H.G. Zhong, P. Beckers, Dual analysis with general boundary conditions, Comput. Methods Appl. Mech. Eng. 122 (1995) 183–192.
[43] M.A. Puso, J. Solberg, A stabilized nodally integrated tetrahedral, Int. J. Numer. Methods Eng. 67 (2006) 841–867.
[44] M.A. Puso, J.S. Chen, E. Zywicz, W. Elmer, Meshfree and finite element nodal integration methods, Int. J. Numer. Methods Eng. (74) (2008) 416–446.
[45] G.R. Liu, T. Nguyen-Thoi, K.Y. Lam, An edge-based smoothed finite element method (ES-FEM) for static and dynamic problems of solid mechanics, J. Sound Vib. 320 (2009) 1100–1130.
[46] P.G. Bergan, C.A. Felippa, A triangular membrane element with rotational degrees of freedom, Comput. Methods Appl. Mech. Eng. 50 (1985) 25–69.
[47] C.A. Felippa, C. Militello, Variational formulation of high-performance finite elements: parametrized variational principles, Comput. Struct. 50 (1) (1990) 1–11.
[48] C.A. Felippa, A survey of parametrized variational principles and applications to computational mechanics, Comput. Methods Appl. Mech. Eng. 113 (1–2) (1994) 109–139.
[49] J.K. Djoko, B.D. Reddy, An extended Hu–Washizu formulation for elasticity, Comput. Methods Appl. Mech. Eng. 195 (2006) 6330–6346.
[50] G.R. Liu, T. Nguyen-Thoi, K.Y. Lam, A novel FEM by scaling the gradient of strains with scaling factor α (αFEM), Comput. Mech., in press, doi:10.1007/s00466-008-0311-1.
[51] G.R. Liu, T. Nguyen-Thoi, K.Y. Lam, A novel alpha finite element method (αFEM) for exact solution to mechanics problems using triangular and tetrahedral elements, Comput. Methods Appl. Mech. Eng. 197 (2008) 3883–3897.
[52] G.R. Liu, H. Nguyen-Xuan, T. Nguyen-Thoi, A variationally consistent alpha FEM (VCαFEM) for nearly exact solution to mechanics problems using quadrilateral elements, Int. J. Numer. Methods Eng., (2009), submitted for publication.
[53] T. Belytschko, W.E. Bachrach, Efficient implementation of quadrilaterals with high coarse-mesh accuracy, Comput. Methods Appl. Mech. Eng. 54 (1986) 279–301.
[54] T. Belytschko, L.P. Bindeman, Assumed strain stabilization of the 4-node quadrilateral with 1-point quadrature for nonlinear problems, Comput. Methods Appl. Mech. Eng. 88 (1993) 311–340.
[55] G.R. Liu, X. Xu, G.Y. Zhang, T. Nguyen-Thoi, A superconvergent point interpolation method (SC-PIM) with piecewise linear strain field using triangular mesh, Int. J. Numer. Methods Eng., in press, doi:10.1002/nme.2464.
[56] T. Belytschko, Y.Y. Lu, L. Gu, Element-free Galerkin methods, Int. J. Numer. Methods Eng. 37 (1994) 229–256.
[57] W.K. Liu, S. Jun, Y.F. Zhang, Reproducing kernel particle methods, Int. J. Numer. Methods Eng. 20 (1995) 1081–1106.

[58] S.N. Atluri, T. Zhu, A new meshless local Petrov–Galerkin (MLPG) approach in computational mechanics, Comput. Mech. 22 (1998) 117–127.
[59] E. Onate, S. Idelsohn, O.C. Zienkiewicz, R.L. Taylor, A finite point method in computational mechanics. Applications to convective transport and fluid flow, Int. J. Numer. Methods Eng. 39 (22) (1996) 3839–3866.
[60] T. Rabczuk, T. Belytschko, S.P. Xiao, Stable particle methods based on Lagrangian kernels, Comput. Methods Appl. Mech. Eng. 193 (12–14) (2004) 1035–1063.
[61] T. Rabczuk, S. Bordas, G. Zi, A three-dimensional meshfree method for continuous crack initiation, nucleation and propagation in statics and dynamics, Comput. Mech. 40 (3) (2007) 473–495.
[62] S. Bordas, T. Rabczuk, G. Zi, Three-dimensional crack initiation, propagation, branching and junction in non-linear materials by an extended meshfree method without asymptotic enrichment, Eng. Fract. Mech. 75 (5) (2008) 943–960.
[63] T. Rabczuk, S. Bordas, G. Zi, On three-dimensional modeling of crack growth using partition of unity methods, Comput. Struct., in press, doi:10.1016/j.compstruc.2008.08.010.
[64] T. Rabczuk, G. Zi, S. Bordas, H. Nguyen-Xuan, A geometrically non-linear three-dimensional cohesive crack method for reinforced concrete structures, Eng. Fract. Mech. 75 (16) (2008) 4740–4758.
[65] M. Fredriksson, N.S. Ottosen, Fast and accurate 4-node quadrilateral, Int. J. Numer. Methods Eng. 61 (2004) 1809–1834.
[66] H. Nguyen-Dang, Finite element equilibrium analysis of creep using the mean value of the equivalent shear modulus, Meccanica 15 (1980) 234–245.
[67] R.H. Macneal, R.L. Harder, A proposed standard set of problems to test finite element accuracy, Finite Elem. Anal. Des. 1 (1985) 3–20.
[68] S.P. Timoshenko, J.N. Goodier, Theory of Elasticity, third ed., McGraw, New York, 1970.
[69] R. Cook, Improved two-dimensional finite element, J. Struct. Div. (ASCE) 100 (1974) 1851–1863.
[70] D. Mijuca, M. Berković, On the efficiency of the primal-mixed finite element scheme, Advances in Computational Structured Mechanics, Civil-Comp Press, 1998. pp. 61–69.
[71] D.P. Flanagan, T. Belytschko, A uniform strain hexahedron and quadrilateral with orthogonal hourglass control, Int. J. Numer. Methods Eng. 17 (1981) 679–706.
[72] D. Kosloff, G.A. Frazier, Treatment of hourglass patterns in low order finite element codes, Int. J. Numer. Anal. Methods Geomech. 2 (1978) 57–72.
[73] P. Beckers, H.G. Zhong, E. Maunder, Numerical comparison of several a posteriori error estimators for 2D stress analysis, Revue Européenne des élémenis finis 2 (1993) 155–178.
[74] K. Bletzinger, M. Bischoff, E. Ramm, A unified approach for shear locking-free triangular and rectangular shell finite elements, Comput. Struct. 75 (2000) 321–334.